



[science.sciencemag.org/content/365/6449/180/suppl/DC1](http://science.sciencemag.org/content/365/6449/180/suppl/DC1)

## Supplementary Materials for

### **Posterior parietal cortex plays a causal role in perceptual and categorical decisions**

Yang Zhou and David J. Freedman\*

\*Corresponding author. Email: [dfreedman@uchicago.edu](mailto:dfreedman@uchicago.edu)

Published 12 July 2019, *Science* **365**, 180 (2019)

DOI: 10.1126/science.aaw8347

#### **This PDF file includes:**

Materials and Methods

Figs. S1 to S19

Tables S1 to S4

References

## Materials and Methods

### *Surgical preparation, Stimuli, and Behavioral Testing*

Two male monkeys (*Macaca mulatta*, 15~16 years old, 8–14 kg) were trained on four different behavioral tasks, and implanted with a head post, and a recording chamber positioned over PPC. Our surgical, behavioral, and neurophysiological approach has been described in detail previously(9, 10). Stereotaxic coordinates for chamber placement were determined from magnetic resonance imaging (MRI) scans obtained before chamber implantation. LIP chambers were centered on the intraparietal sulcus (IPS), 4.0 mm posterior to the intra-aural line and 1.0 mm lateral from the midline for monkey M, and 0 mm anterior to the intra-aural line and 15.0 mm lateral from the midline for monkey B. Monkeys were housed in individual cages under a 12 hours light/dark cycle. Behavioral training and experimental recordings were conducted during the light portion of the cycle. Monkeys sat comfortably while head-fixed in a custom-made primate chair inside a dark experiment rig. Task stimuli were displayed on a 21-inch color CRT monitor (1280\*1024 resolution, 75 Hz refresh rate, 57 cm viewing distance). Identical stimuli, timing, and rewards were used for both monkeys. A solenoid-operated reward system was used to deliver juice reward to the monkeys. Monkeys' eye positions were monitored by an optical eye tracker (SR Research) at a sampling rate of 1 kHz and stored for offline analysis. Stimulus presentation, task events, rewards, and behavioral data acquisition were accomplished using an Intel-based PC equipped with MonkeyLogic software running in MATLAB (<http://www.monkeylogic.net>)(36). All experimental and surgical procedures were in accordance with the University of Chicago Animal Care and Use Committee and National Institutes of Health guidelines.

### *Behavioral tasks*

#### *Motion direction categorization task (MDC)*

On each trial, monkeys were required to saccade to either the green or red targets based on the category of the motion stimulus. Ten motion directions ( $55^\circ$ ,  $75^\circ$ ,  $135^\circ$ ,  $195^\circ$ ,  $215^\circ$ ,  $235^\circ$ ,  $255^\circ$ ,  $315^\circ$ ,  $15^\circ$ ,  $35^\circ$ ) were grouped into two categories separated by a learned category boundary (**Fig. 1B**). Task difficulty was determined by the angular distance between the direction of motion and the boundary. A trial was initiated by the monkey holding a touch-bar and acquiring gaze fixation. Monkeys needed to maintain fixation within  $2.0$ - $2.5^\circ$  radius of a fixation point throughout the trial, prior to their saccadic choice. After a 500 ms fixation period, two colored saccade targets (red and green) appeared simultaneously at opposite positions relative to the fixation point with equal eccentricities ( $8^\circ$  and  $9^\circ$  for Monkey M and B, respectively). The positions of red and green targets were randomly chosen between the two positions on each trial(37). 400ms later, a sample motion stimulus was presented at a location orthogonal to the axis of, but at the same eccentricity as, the saccade targets. The motion stimuli were full contrast,  $8^\circ$  diameter, 100% coherent, random-dot movies composed of 190 dots per frame, and moved at  $10^\circ$ /s. Monkeys needed to saccade to either red or green targets within a 60-2000ms window after sample stimulus onset. If the sample stimulus belonged to category one ( $55^\circ$ ,  $75^\circ$ ,  $135^\circ$ ,  $195^\circ$ ,  $215^\circ$ ), the monkey needed to saccade to green target, whereas category two ( $235^\circ$ ,  $255^\circ$ ,  $315^\circ$ ,  $15^\circ$ ,  $35^\circ$ ) was associated with the red target. If the monkey's saccade brought its gaze to within a  $3^\circ$  window around the correct target and held for 100 ms, a juice reward was delivered.

### *Motion direction discrimination task (MDD)*

Monkeys needed to choose either the green or red saccade targets based on motion direction of the sample stimulus. The timings and spatial positions of the saccade targets and motion stimuli were the same as in MDC task. Two motion directions ( $135^\circ$ ,  $315^\circ$ ) with three different coherence levels (9%, 18%, 36% for monkey M; and 13%, 25%, 50% for monkey B) were used in this task. Task difficulty was determined by the coherence level of the motion stimuli, defined as the percentage of dots moving coherently in one direction. The direction of motion for each non-coherent (i.e. noise) dot was chosen randomly, and each moved in a consistent direction across all video frames. If the sample direction was  $135^\circ$ , the monkey needed to saccade to the green target to receive a juice reward, whereas the  $315^\circ$  direction was associated with the red target. The same timings and stimuli were used for both inactivation and recording sessions except that zero coherence stimuli were also used during recording sessions. On each zero coherence trial, the rewarded target (red or green) was randomly (50% probability) chosen.

### *Free saccade choice task (FSC)*

A free saccade choice task was used to assess the effectiveness of LIP inactivation and its impact on saccade selection, as demonstrated by previous studies (16, 23, 28) (**Fig. S19**). Both monkeys performed this task at the start of each control and inactivation session. Monkeys were trained to freely choose between two visually identical saccade targets. Trials were initiated when the monkey grasped a touch-bar, and maintained gaze fixation (within  $2.0$ - $2.5^\circ$ ) of a central fixation spot. After a 500 ms fixation period, the central fixation point disappeared, and two red saccade targets appeared either simultaneously or sequentially for 60ms, at opposite directions relative to the fixation point and with equal eccentricities ( $8^\circ$  and  $9^\circ$  eccentricity for Monkey M and B, respectively). On each trial, target onset asynchrony was randomly chosen from seven different values with equal probability (left target relative to right target, -120ms, -80ms, -40ms, 0ms, 40ms, 80ms, 120ms). The monkeys were free to saccade to either the left or right targets immediately. On each trial, the reward probability for each target was determined independently and at random. A higher reward probability was used for the earlier than later appearing target (0.85 vs. 0.6), in order to motivate the monkey to saccade to the earlier target (rather than employing a fixed side bias). On 20% of trials, only a single target appeared, and monkeys needed to saccade to its position. Reward probability on single target trials was equal to that of the earlier appearing target in the two target trials.

### *Memory guided saccade task (MGS)*

A memory guided saccade task was used to identify LIP neurons and to map their RFs. Trials were initiated by the monkey grasping the touch-bar lever and maintaining central fixation. After the 500 ms fixation period, a visual target was shown for 200ms at one of eight possible locations, evenly placed at  $45^\circ$  angular positions with eccentricity ranging from  $6^\circ$  to  $12^\circ$ . Following stimulus offset, monkeys maintained central fixation for 1s at which time the fixation point disappeared. They then had to make a single saccade toward the remembered target location within 500 ms, and fixate that location for 200 ms in order to receive a juice reward.

### *Stimulus and target configurations in the MDC and MDD tasks*

To test LIP's causal involvement in the sensory evaluation and motor planning aspects of decisions, we arranged the saccade targets and motion stimulus in three different spatial configurations in different blocks of trials (**Fig. 1C** and see below). Before the inactivation

sessions, we recorded LIP neurons' activity in MGS task, and mapped their RF positions. We found a coarse retinotopic map from the anterior to posterior LIP in both monkeys, corresponding to upper-contralateral to lower-contralateral visual field. For each inactivation session, we targeted muscimol injections to LIP locations from which most of the recorded neurons showed either visually-driven or persistent activity to the visual target in the middle-contralateral VF within a 6°-12° eccentricity range. The middle-contralateral VF was therefore defined as the inactivated visual field (IVF). The three spatial task configurations were defined according the spatial positions of targets and motion stimuli relative to the IVF (**Fig. 1C**). 1) In the stimulus-In ( $S_{IN}$ ) condition, the motion stimulus was presented inside the IVF, but the saccade targets were directly above and below the fixation point and outside the IVF. In the  $S_{IN}$  condition, muscimol injection into LIP examines the impact of inactivation on sensory evaluation of the in-RF motion stimulus. 2) In the Target-In ( $T_{IN}$ ) condition, the two saccade targets were presented in the IVF and the ipsilateral visual field, respectively, while the motion stimulus was presented directly above the fixation point at the same eccentricity as the saccade targets. In  $T_{IN}$ , muscimol injection into LIP examines the impact of inactivation on saccade selection. 3) In the Both-Out ( $B_{OUT}$ ) condition, the motion stimulus was presented in the ipsilateral VF (opposite to the IVF) at the same eccentricity as the  $S_{IN}$  condition, and the saccade targets were in the same positions as the  $S_{IN}$  condition. In  $B_{OUT}$ , LIP inactivation is not expected to strongly influence sensory evaluation or saccade selection since both the motion stimuli and saccade targets are outside the IVF. Thus  $B_{OUT}$  is used as a within-session control condition to monitor monkeys' general behavioral state after LIP inactivation, assessing factors such as the animals' motivation and arousal. The stimulus configuration was fixed within each block and the order and duration of the three condition blocks is described below. The exact same stimulus spatial configurations were used on inactivation and control sessions.

#### *Task sequence on each session*

For each experiment session, monkeys were first tested with the FSC task for ~15-20 minutes (~250 trials), and then tested on the MDC and MDD tasks. There were three different blocks for both MDC and MDD tasks which tested performance in each of the 3 spatial configurations of stimuli and saccade targets (**Fig. 1C**). The six experiment blocks (3 conditions  $\times$  2 tasks) were randomly interleaved without replacement within each session. The MDC and MDD tasks were cued by different fixation point colors, with blue for MDC task and yellow for MDD task. In each block, monkeys needed to perform 60-110 (Monkey M: 60 for MDD and 100 for MDC; Monkey B: 70 for MDD and 110 for MDC) correct trials before advancing to the next block. On inactivation sessions, monkeys were typically tested with the FSC task 30 minutes after the completion of muscimol infusion; while during the control sessions, monkeys needed to wait for an equivalent duration as during the inactivation session before performing the FSC task.

#### *Muscimol infusion*

The GABA<sub>A</sub> agonist muscimol (Sigma) was dissolved in phosphate-buffered saline (PBS), pH  $\approx$  7, to concentrations of about 8  $\mu$ g/ $\mu$ l. We infused the muscimol solution into the cortex using a similar approach as a recent study(16). On each session, two infusion cannulas were lowered into grid locations and depths in which we had previously recorded LIP neurons with RFs located in the middle-contralateral VF. The two cannulas (32 gauge) were lowered by motorized micro-drives (NAN Instruments) with a 1-3 mm separation within the grid. Infusions were

performed using a syringe pump (Harvard Apparatus) using a 10  $\mu\text{l}$  micro-syringe (Hamilton) and polyethylene tubing (PE20, inner diameter = 0.38 mm, outer diameter = 1.09 mm) directly connected to the cannula. We delivered 6-8  $\mu\text{l}$  (3-4 for each cannula) of muscimol solution in each inactivation session, corresponding to a total drug delivery of  $\sim 50 \mu\text{g}$  (mean = 53.4  $\mu\text{g}$ ) of muscimol. This protocol was chosen to match the high end of ranges used previously in order to maximize neural inactivation. To avoid pressure damage and maximize the inactivated cortical area, muscimol solution was infused at five different depths along a single cannula track. For each infusion depth, we infused 0.5-0.8  $\mu\text{l}$  muscimol solution (constant rate of 0.2  $\mu\text{l}/\text{min}$ , 2.5-4 minutes), and the injection cannula stayed at that depth for at least 2 minutes after finishing infusion. For each infusion site, we visually monitored the movement of the solution to make sure that the drug was successfully delivered. It typically took 40-50 minutes to finish the infusion process. Cannula were left at the last infusion depth in the cortex during the remainder of the session. Behavioral testing started  $\sim 30$ -35 minutes after completing the muscimol infusion, and typically concluded within 2.5-3.5 hours following infusion. As monkeys sometimes showed a saccade choice bias toward the ipsilateral target in the FSC task one day following an inactivation session, control data sessions were obtained on one day before and two days after an inactivation session, using precisely the same tasks, stimuli and parameters as during the inactivation session. In two sham control sessions, saline was infused into LIP using the same methods as muscimol infusion. The injection location and the volume was the same between sham control and inactivation sessions. The monkeys' behavioral performance on sham control sessions was very similar as control sessions, although the small number of sham sessions precludes statistical analysis. We elected not to conduct more sham controls, to limit cortical damage due to needle insertion and fluid injection.

### ***Electrophysiological recording***

Neuronal activity was recorded using 75- $\mu\text{m}$  tungsten microelectrodes (FHC,  $\sim 1 \text{ M}\Omega$ ), or 16-channel V-Probes (Plexon). All neurons from monkey M were recorded using single channel electrode, and most neurons from monkey B were recorded using V-probes (16 recording sites in one row, 100  $\mu\text{m}$  inter-site spacing). Neurophysiological signals from both single or multi-channel recording were amplified, digitized and stored for offline spike sorting (Plexon) to verify the quality and stability of neuronal isolations. For both monkeys, we recorded neuronal activity in MGS task to map LIP RF locations before we commenced with the first inactivation session. Neuronal recordings on the MDD task were conducted in Monkey M after the inactivation sessions, while MDD task data was recorded from monkey B before the inactivation sessions.

We localized LIP in each monkey according to the pattern of neuronal activity, particularly during the MGS task (e.g. spatially selective activity during stimulus presentation and the delay). All neurons included in the dataset were recorded from the same grid holes and similar depths ( $\sim 5$ -10 mm from the cortical surface) where we encountered spatial selectivity in the MGS task. LIP neurons were also identified based on anatomical criteria, such as the location of each electrode track relative to that expected from the MRI scans, the pattern of gray-white matter transitions encountered on each electrode penetration, and the relative depths of each neuron.

To test whether the inactivation-related behavioral deficit in the  $S_{\text{IN}}$  condition was due to impairment of decision-related activity (as opposed to other factors such as attention or visual feature encoding), we recorded LIP neurons' activity in the  $S_{\text{IN}}$  condition of the MDD task. For

single channel electrode recording, only neurons showing visual responses to the motion stimuli during prescreening with the MDD task were tested with ~300-600 trials of the MDD task. For neurons with clear spatial RFs during the MGS task, we presented motion stimulus inside LIP neurons' RF; while for those neurons which did not show a clear RF during the MGS task, we presented motion stimuli in the positions (always in the visual field contralateral to the recorded hemisphere) in which neurons exhibited the strongest response to the motion stimuli. For the multi-channel recordings, we recorded all neurons isolated across all channels, with the motion stimulus placed in one of the isolated neurons' RFs. Because adjacent recording sites were located 100 $\mu$ m apart, nearby neurons typically had similar RF locations.

## *Data analysis*

### *Behavioral performance*

Only sessions in which monkeys performed enough trials for each unique stimulus condition in both the MDC and MDD tasks ( $n \geq 20$  for monkey M and  $n \geq 30$  for monkey B) were used for further analysis. For monkey M, we collected data from 10 inactivation sessions in total. However, two inactivation sessions were excluded from further analysis as the infusion cannula was clogged in one inactivation session, and monkey M did not perform enough trials (less than half of the required number) in the other excluded session. We used the session before and the session two days after each inactivation session as controls. This gave a total of 11 control sessions and 8 inactivation sessions for monkey M. For monkey B, we collected data from 11 inactivation sessions, and 12 control sessions. However, two inactivation sessions were excluded from analysis in which the injection cannula was clogged or was later determined to have missed the target location of LIP based on MRI images and electrophysiological mapping, respectively. Furthermore, the final control session was excluded from data analysis, as the monkey worked fewer trials and with much lower overall performance (e.g. more fixation breaks, aborted trials, and lower accuracy) than on typical control sessions. Therefore, there are 11 control sessions and 9 inactivation sessions from monkey B included for analysis. On average, monkey M performed 1314 trials per session, and monkey B performed 2038 trials per session (including both correct and error trials in the MDC and MDD tasks).

We only included trials for analysis in which monkeys made a saccade directly to one of the two targets, while fixation-break and aborted trials were excluded. We included both correct and error trials for calculating monkeys' mean RT for every experiment condition. To facilitate pooling of the two monkeys' data, we defined the primary category/direction for each monkey as the category/direction for which the monkey showed a greater deficit in the  $S_{IN}$  condition on average across all inactivation sessions, since both animals showed greater inactivation-related deficits for one of the two categories. In the  $S_{IN}$  and  $B_{OUT}$  conditions, we pooled data from the two monkeys based on the "primary" category/direction of each monkey. Trials from different saccade directions are pooled for each category. In the  $T_{IN}$  condition, data from two monkeys were pooled according to the saccade target location relative to the inactivated hemisphere. Trials in  $T_{IN}$  were grouped based on saccade direction (ipsilateral vs. contralateral). Trials from both categories were pooled for each target location.

### *Psychometric curve fitting*

We used a cumulative Gaussian function to fit psychometric curves to performance in the MDC and MDD tasks, using the maximum likelihood method. In the  $S_{IN}$  and  $B_{OUT}$  conditions, we calculated the proportion of trials for choosing the primary category/direction as a function of motion category/direction with different task difficulty levels (negative values represent ‘non-primary category/direction’; positive values represent ‘primary category/direction’). In the  $T_{IN}$  condition, we calculated the proportion of trials for choosing the contralateral target as a function of motion category/direction with different task difficulty levels (negative values represent ‘ipsilateral target’; positive values represent ‘contralateral target’). There are two free parameters: (1) the psychophysical threshold was taken as the SD of the Gaussian fit and corresponded to 84.15% correct performance, and (2) the point of subjective equality (bias) was taken as the mean of the Gaussian fit, corresponding to the stimulus conditions that yielded 50%-50% primary vs non-primary category/direction choices in both  $S_{IN}$  and  $B_{OUT}$  conditions, or the stimulus conditions that yielded 50%-50% contralateral vs ipsilateral saccade choices in the  $T_{IN}$  condition. In **Fig. 2, M to P** and **Fig. 3, M to P**, the values of each paired control session were defined as the mean value of the results from the sessions both before and after the corresponding inactivation session.

#### *Drift-diffusion model fitting*

The drift diffusion model has been widely used for modelling behavior during decision making in two-choice discrimination (decision) tasks, as it translates behavioral data, including both accuracy and reaction time (RT) distributions, into distinct components such as bias, sensitivity and threshold(38, 39). To test which components of the decision-making process were impaired by LIP inactivation in different task conditions, we fit the monkeys’ behavioral data in both control and inactivation sessions, to drift diffusion models with fixed boundaries (**figs. S6 and S7**). In these models, noisy sensory evidence is assumed to accumulate over time from a starting point ( $\mathbf{z}$ , representing choice bias) toward one of two decision boundaries (0 and  $\mathbf{a}$ , representing the decision threshold). The rate of evidence accumulation is the drift rate ( $\mathbf{v}$ ) and is determined by the strength of sensory evidence (angular difference between the motion direction and the category boundary in the MDC task, and the motion coherence in MDD task). We also assume across-trial variability ( $\boldsymbol{\eta}$ ) in the accumulation of evidence. This corresponds to the variability of drift rate between different trials, potentially due to noise from early sensory processing, or variability in attention or motivation. Factors less directly related to decisions, such as sensory feature encoding and motor control, also contribute to subjects’ RTs during decision tasks. Thus, a uniformly distributed non-decision RT which accounts for all non-decision processes involved (with mean  $\mathbf{T}_{er}$  and std  $\mathbf{s}_t$ ) is also used to fit the RT distributions. The value of the starting point of the diffusion process also varies from trial to trial (std  $\mathbf{s}_z$ ) in the current model, which is shown to be important for explaining RT differences between correct and error trials(40). Furthermore, we used quantiles rather than mean RTs for both correct and error trials, in order to increase statistical power. We used a MATLAB (Mathworks Inc) based library (Diffusion Model Analysis Toolbox – DMAT(41)), to fit the 7 parameters listed above using both accuracy and RT data in each task condition.

We fit each monkey’s behavioral data in each condition (three spatial configurations in two tasks, six conditions in total) independently for both inactivation and control sessions. Six of the seven parameters were freely fit with one fixed value for all the task difficulty levels within a given task condition, as we assume the bias, threshold and non-decision time are fixed within each task

condition for each subject. The drift rate ( $\mathbf{v}$ ) was fit freely for each task difficulty level in each task (**Tables S1-S4**).

#### *Saccade analysis:*

We detected saccades using a threshold for velocity and template-matching criteria as in previous studies(42, 43). Horizontal and vertical eye positions, sampled at 1000 Hz, were used to calculate the instantaneous eye movement velocity. Velocity vectors were smoothed (20 ms boxcar) to reduce noise. The start of a saccade was defined as the time when the velocity exceeded  $30^\circ/\text{s}$ , and the end of a saccade was defined as the first point at which the velocity was less than 10% of the peak velocity. Furthermore, trials were only included for further analysis if they fit the following criteria: (1) the saccade duration was 10 to 100 ms; (2) the saccadic endpoint was within a  $5^\circ$  window that was centered at the saccade target; (3) the saccade amplitude was no less than half of the eccentricity of the target (typically  $4.5^\circ$ ). To whether LIP inactivation produced an obvious impairment of eye movements, we compared monkeys' peak saccade velocity between control and inactivation sessions (**fig. S10**). Only data from the  $T_{\text{IN}}$  condition in which one of the saccade targets was placed in the inactivated visual field were included in this analysis.

#### *Microsaccade analysis*

We detected monkeys' micro-saccades based on velocity criteria similar to previous studies(44, 45). Horizontal and vertical eye positions, sampled at 1000 Hz, were used to calculate an instantaneous eye movement velocity. Velocity vectors were smoothed (20 ms boxcar) to reduce noise. We then used the following criteria to detect micro-saccades: (1) the eye movement velocity  $> 10 \text{ deg/s}$ ; (2)  $10 \text{ ms} < \text{eye movement duration} < 100 \text{ ms}$ ; (3) eye movement amplitude  $\geq 0.05$  degree; (4) a new micro-saccade could not be initiated within 20 ms of a previous micro-saccade. Furthermore, a 'rate-of-turn' criterion--the saccade direction could change no more than 30 degrees every 5 ms during the micro-saccade—was also used to determine the end of micro-saccades. Visual inspection of raw eye movement traces was used to confirm the accuracy of this micro-saccade detection. For **fig. S7**, we only analyzed the micro-saccades within a time window following target onset and before motion stimulus onset, as we expect that the monkeys' micro-saccades were less influenced by factors such as visual stimulus onset and saccade preparation in this period, compared to the later sample period (making it more likely to detect a bias). The same micro-saccade analysis during other tasks periods produced similar results.

## **Neuronal data analysis**

#### *Neuronal pre-screening*

All neurons recorded from single channel electrodes were included for analysis. For multi-channel recordings, we only included the neurons which showed significant modulation (different from fixation period activity, one-way ANOVA,  $p < 0.01$ ) of their averaged activity across all motion stimuli as the stimulus could not always be placed within the RF of all the neurons recorded by the linear array. We also excluded the neurons with maximum firing rates  $< 2.0$  spikes/s (to the direction producing greater average responses) during stimulus presentation. To select neurons that showed significant motion direction selectivity (DS) during the decision period, we applied a one-way ANOVA test to compare activity between the two different motion directions in the

period following motion stimulus onset (50-250 ms after motion stimulus onset). Only neurons that showed significant ( $p < 0.01$ ) DS were used for further analysis.

#### *Spike density function and normalized activity*

For all plots showing the single neuron and population activity, we used a 20 ms Gaussian smoothing window for each neuron. For population plots, we normalized each neuron's activity by its maximum firing rate (averaged across all conditions) across the trial (from fixation onset to 1100 ms after motion onset).

#### *Receiver operating characteristic (ROC) analysis*

We applied a sliding ROC analysis (100 ms width, 5 ms steps) to the distribution of firing rates to quantify each neuron's DS in the MDD task. The area under the ROC curve is a value between 0.0 and 1.0 indicating the performance of an ideal observer in assigning motion direction based on each neuron's trial-by-trial firing rates. Values of 1.0 and 0.0 correspond to perfect classification (i.e. strong DS), while a value of 0.5 indicates chance classification performance (i.e. no DS). For trials with zero coherence motion, we assigned direction labels on each trial according to the monkey's choice. To test whether DS reflected monkeys' trial-by-trial choices, we used an ROC analysis to quantify whether LIP activity was more correlated with monkeys' trial-by-trial choices than the physical direction of stimulus motion, by analyzing both correct and error trials. Only low coherence trials, which had sufficient numbers of error trials (average performance: Monkey M: 74% correct, Monkey B: 67% correct), were included in this analysis. LIP neuronal activity was analyzed by ROC according to either monkey's trial-by-trial choices or the direction of sample stimulus on each trial. Only neurons for which we recorded sufficient trials ( $>4$ ) for the low coherence condition of each motion direction were used for this analysis ( $N=101/104$ ). In **Fig. 4, G,H**, trials from each saccade direction were separated into the faster-half and slower-half RT sub-groups for each coherence level, and then pooled for each motion direction.

#### *Selectivity latency*

For each neuron, a one-way ANOVA was applied to the distributions of firing rates to the both motion directions using a sliding window (50ms window width, 10ms steps) to determine the latency of DS. We defined the middle time point of the first time window for which there was significant difference ( $p < 0.01$ ) between neuronal responses to the two directions in three successive time windows. Only correct trials with non-zero coherence motion were used for this analysis.

#### *Correlation between direction selectivity and RT*

In order to test the correlation between the motion direction selectivity of LIP neurons and monkeys' RTs, we show LIP population activity grouped in different RT bins (**fig. S15**). For each neuron, we separated the trials of each motion direction into six equal size groups. First, we separated the trials with the same motion direction into two sub-groups based on their saccade direction. In this way, we lessened the possibility that the two saccade directions differentially influenced neuronal activity in the respective RT bins. Trials with the same motion direction and same saccade direction were grouped into six bins according to the monkey's RT from low to high. Next, bins from the two different saccade directions but same motion direction were pooled based on RT (1 to 6 from low to high). Neuronal activity within each RT bin was averaged for each motion direction, and then pooled across the population based on each neuron's preferred and non-

preferred direction. All neurons contributed equally to the population activity of each RT bin. Similar procedures were performed for different RT bins in other figures (two RT bins in **Fig. 4, G,H** and **fig. S14**).

To test the correlation between the slope of LIP responses and the monkeys' RT, we quantified the slope of LIP neurons' averaged population differential activity (the difference in activity between preferred and non-preferred directions). The differential activity was first calculated for each neuron and then pooled together across the population. To calculate the slope value, we first identified the starting time of the onset of ramping differential activity. The start point was defined as the first time point at which the differential activity exceeds three times the standard deviation of the baseline differential activity, and for which the following 100ms keeps increasing. Then, we linearly regressed the differential activity in a 100 ms window following the start point to determine a value for the slope of the ramping activity.

#### *Partial correlation analysis*

A partial correlation analysis was performed similar as in a previous study(19). For each trial of the MDD task, we obtained three parameters, i.e., the stimulus direction, the pre-choice neuronal activity, and the monkeys' choice, for the calculation. The stimulus directions are assigned different values for different directions and coherence levels: positive and negative values are used for 315° and 135°, respectively; while 4, 2, 1 and 0 are used for code the high, middle, low and zero coherence levels. Different choice directions are also coded as different values (-2 for choosing 135°, and + 2 for choosing 315°). Two measures were then calculated:  $r_{\text{stimulus}} = r(\text{neuronal activity, stimulus direction} | \text{choice direction})$ , the partial correlation between neuronal activity and stimulus direction, given the monkeys' choices; and  $r_{\text{choice}} = r(\text{neuronal activity, choice direction} | \text{stimulus direction})$ , the partial correlation between neuronal activity and monkeys' choice, given the stimulus direction. In **Fig. 4J**, the neuronal activity was chosen as the average firing rate of each neuron in a 100 ms immediately prior to the monkey's choice. In **Fig. 4I** and **S16**, the neuronal activity for each neuron was the average firing rate in a 50ms window, advanced in 10 ms steps.

#### *Site by site comparison of neuronal selectivity and behavioral impact of inactivation:*

We tested the relationship between the behavioral impacts arising from LIP inactivation and the neuronal selectivity of LIP neurons in the inactivated sites by comparing the pattern of behavioral deficits with the direction/category preferences of neurons at each inactivated LIP site. We tested whether the majority of LIP neurons recorded at each inactivation site showed stimulus preferences which corresponded with the behavioral deficits observed when inactivating those sites. This also serves as an analytical control to ensure that our results were not driven by our method for determining the primary direction/category for each monkey (the direction/category for which behavior was more impacted by inactivation). However, note that the inactivation results are shown separately for each monkey without the step of determining the primary category/direction (**figs. S4** and **S5**), showing results which were consistent (and statistically significant) with the combined data.

Monkey M showed a clear neuronal selectivity bias in each of the four grid positions from which we recorded (and inactivated) LIP, with the overwhelming majority of recorded neurons (39 of 50) preferring one of the two directions (315°). This selectivity bias was also evident by plotting the population activity pooled in a global manner according to the global preferred (315°)

and non-preferred ( $135^\circ$ ) directions (**fig. S17 A,B**). The preferred direction of those sites happened to correspond with the primary direction (i.e. the direction for which behavior was more affected by inactivation on average across all sessions, see **fig. S4**). In other words, the primary direction for this monkey is the same when defined as either the direction for which behavior was more strongly affected by inactivation, or when it was defined by the preferred stimulus direction of the targeted LIP sites. Thus, for Monkey M, the results are consistent with inactivation preferentially impairing behavior for the categories/directions corresponding with the selectivity preferences of neurons at the site of inactivation.

Monkey B did not exhibit a global bias in category/direction preference, but instead showed a more balanced preference across the population ( $135^\circ$ : n=28 neurons;  $315^\circ$ : n=26 neurons). However, when we examined the specific sites (grid locations) from which we recorded and inactivated, we found that individual sites showed more consistent preferences for one or the other direction. Five of the sites contained more neurons which preferred one of the directions (24 of 39 neurons preferred  $135^\circ$ ), which corresponded to the primary category/direction determined based solely on the average behavioral impact of inactivation (see **fig. S5**). The other two sites contained more neurons which responded preferentially to the opposite (non-primary) direction (11 of 15 neurons preferred  $315^\circ$ ). We next examined how inactivation of those two sites impacted behavior. This revealed a (non-significant) trend toward greater impairment for the direction which corresponded to the preferences of the neurons at those two sites which preferred the non-primary direction. For this monkey, we redefined the primary and non-primary categories/directions according to the preferences of neurons at each recording site. In **fig. S17, C,D**, we re-plotted the population activity based on these new primary/non-primary labels. **Fig. S18** shows the behavioral effects of inactivation for Monkey B, with the red trace showing the results when defining the primary category/direction according to the neuronal preference at each inactivation site. The black trace shows the same data with the primary category/direction defined globally according to the average behavioral impact on performance across all inactivation sessions (as in **Fig. 2**). For the MDC task, the results are indistinguishable from the original method for defining the primary category. For the MDD task, there is a trend (non-significant) toward greater behavioral impairments for the primary direction when taking into account each site's stimulus preference. A caveat is that in our inactivation experiments, we inactivated two sites simultaneously, occasionally including one site which preferred the primary category/direction, and one site which preferred the opposite. We included these sessions in the "non-primary" group in the above analysis.

## Supplementary Figures

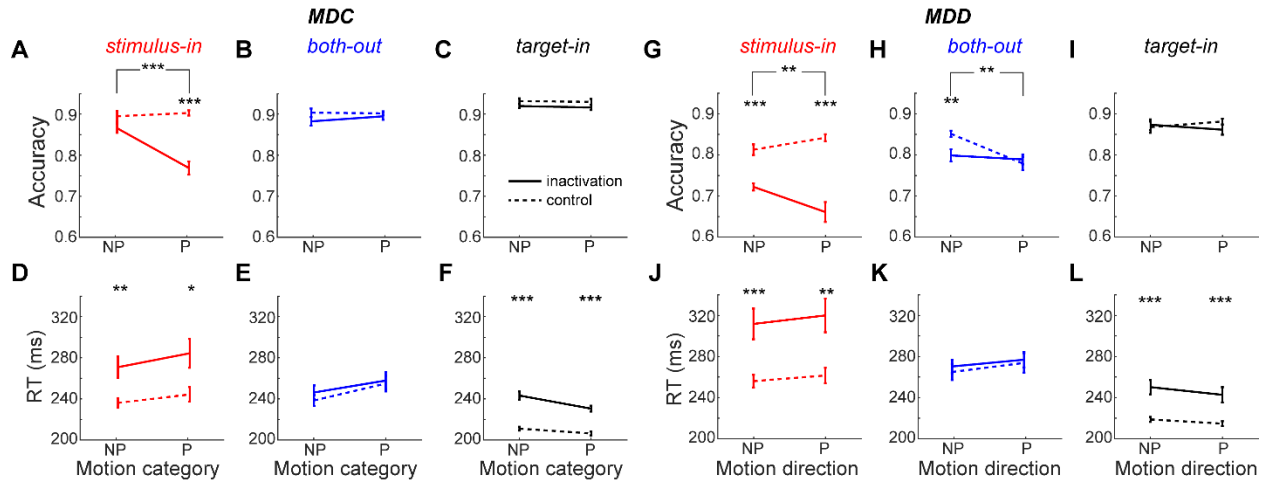


**Fig. S1.**

Comparisons of behavioral deficits between different categories/directions. Left panels: monkeys' behavioral performance in the MDC task. (A-C) Monkeys' accuracy in  $S_{IN}$  (A),  $B_{OUT}$  (B) and  $T_{IN}$  (C) conditions of the MDC task, shown separately for inactivation and control sessions. Data from both monkeys were pooled based on the primary and non-primary categories of each monkey. A larger decrease in accuracy was observed for the primary category compared to the non-primary category in  $S_{IN}$  condition. (D-F) Monkeys' mean RT in the three MDC task conditions. Right panels: monkeys' behavioral performance during the MDD task. (G-I) Monkeys' accuracy in the three conditions of the MDD task, shown in the same format as in (A-C). A larger decrease in accuracy was observed for the primary direction compared to the non-primary direction in  $S_{IN}$  condition. (J-L) Monkeys' mean RT in the three conditions of the MDD task. Note that trials in all panels were grouped based on the categories/directions of the motion stimuli.

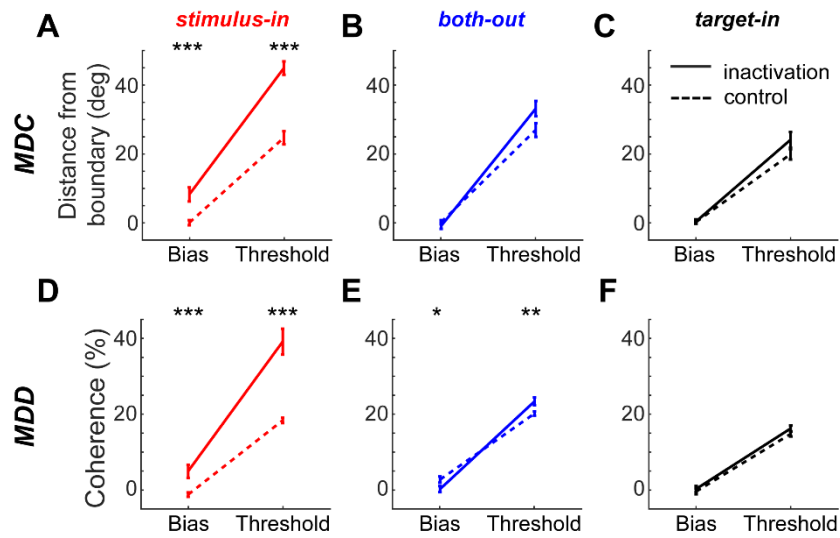


**Fig. S2.**

Choice bias and psychophysical threshold following LIP inactivation. Choice bias and psychophysical threshold were estimated by fitting the monkeys' psychometric curves with cumulative gaussian functions. (A-C) The resulting values for choice bias and psychophysical threshold in  $S_{IN}$  (A),  $B_{OUT}$  (B) and  $T_{IN}$  (C) conditions of the MDC task are shown separately for inactivation and control sessions. The psychometric curves for both monkeys were pooled according to the primary categories before curve fitting. LIP inactivation resulted in a change in choice bias and an increase in psychophysical threshold in  $S_{IN}$  condition. (D-F) The resulting values for choice bias and psychophysical threshold in the three conditions of the MDD task are shown in the same format as in (A-C).

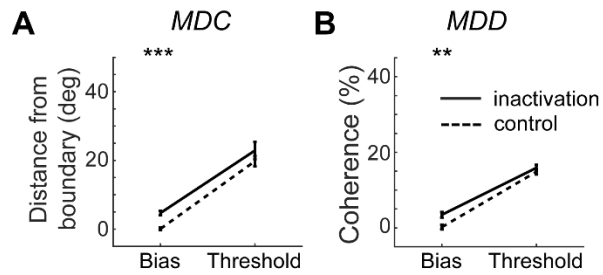


**Fig. S3.**

Impact of LIP inactivation on saccade choice bias and psychophysical threshold in  $T_{IN}$  conditions. Trials were grouped based on the target location. The psychometric curves from both monkeys were pooled according to the contralateral saccade directions before curve fitting. The resulting values for choice bias and psychophysical threshold in  $T_{IN}$  conditions in the MDC (A) and MDD (B) tasks are shown separately. Only saccade choice bias but not psychophysical threshold in the  $T_{IN}$  condition were affected by LIP inactivation in both tasks.

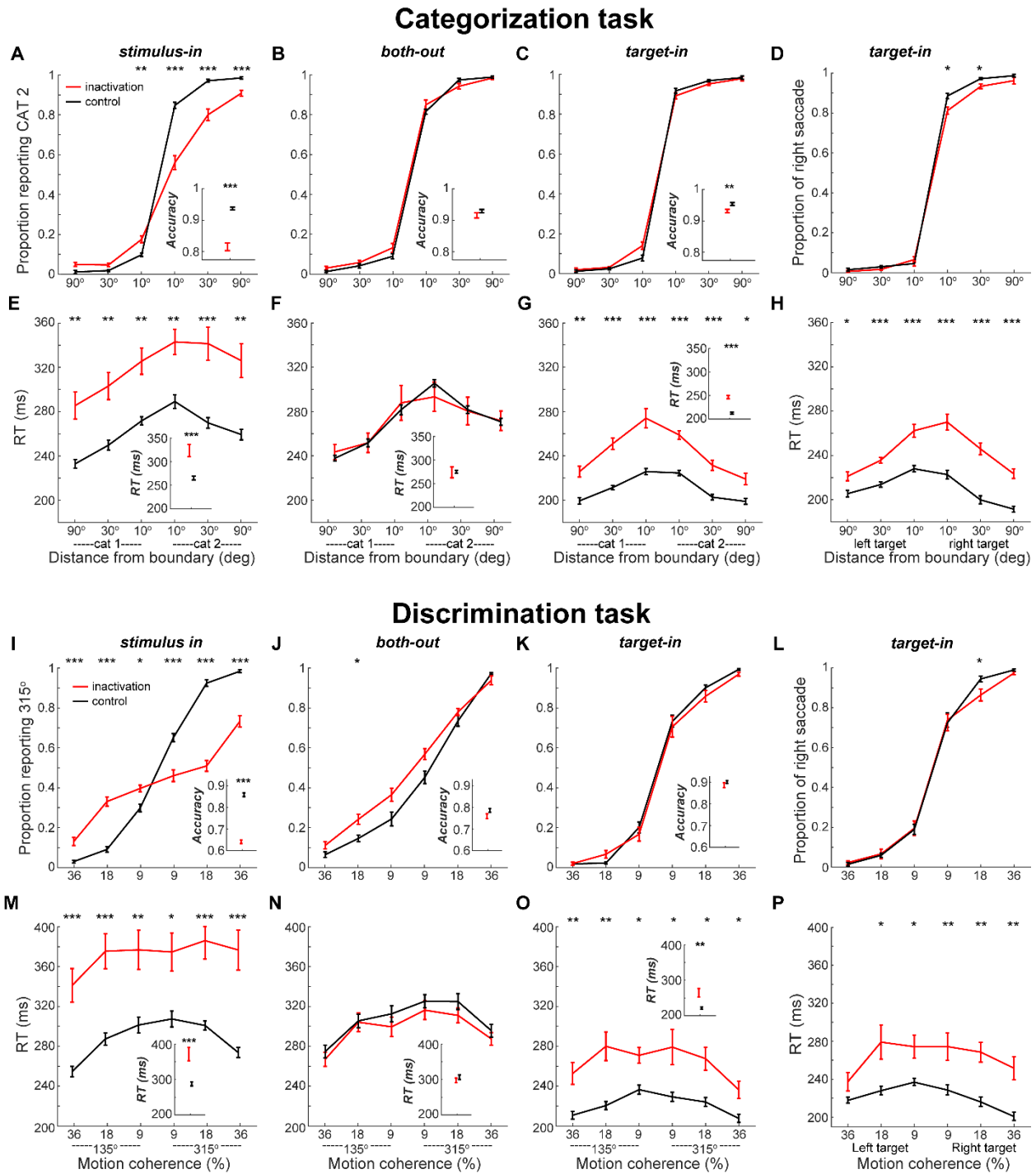


**Fig. S4.**

Behavioral performance of monkey M on inactivation and control sessions. Upper panels: Behavioral performance in MDC task. (A-C) Psychometric curves in  $S_{IN}$  (A),  $B_{OUT}$  (B) and  $T_{IN}$  (C) conditions in MDC task, shown separately for inactivation and control sessions. The choice accuracy was plotted as the proportion of choosing category 2 (red target). Trials from different saccade directions but the same difficulty level (angular distance from the boundary) were grouped for each category. Note that monkey M exhibited a larger decrease in accuracy for category 2 than

category 1 in the  $S_{IN}$  condition. Therefore, category 2 was defined as the primary category for monkey M. **(D)** Psychometric curves in  $T_{IN}$  conditions for which the trials were grouped based on the target location (same data as **C**). Choice accuracy is plotted as the proportion of rightward saccades. Trials of the same difficulty level from both categories were grouped for each target location. The monkey's saccade choice was biased away from the IVF (right visual field, the left hemisphere of monkey M was inactivated). **(E-G)** Chronometric curves for  $S_{IN}$  (**E**),  $B_{OUT}$  (**F**) and  $T_{IN}$  (**G**) conditions in the MDC task. **(H)** Chronometric curves in  $T_{IN}$  condition in MDC task, for which trials were grouped based on target location. The inset figure in each panel shows the global performance in each condition. The black stars indicate the statistical significance for the comparisons between control and inactivation sessions (\*:  $p < 0.05$ , \*\*:  $P < 0.01$ , \*\*\*:  $p < 0.001$ , unpaired t-test, multiple tests are Bonferroni corrected). The error bars denote  $\pm SEM$ . Lower panels: Behavioral performance in MDD task. **(I-K)** Psychometric curves in three conditions of the MDD task. The choice accuracy is plotted as the proportion of choosing  $315^\circ$  (red target, center direction of category 2). Trials from different saccade directions but same difficulty level (coherence) were grouped for each motion direction. Note that monkey M exhibited a larger decrease in accuracy for  $315^\circ$  than  $135^\circ$  stimuli in the  $S_{IN}$  conditions. Therefore,  $315^\circ$  was defined as the primary direction for monkey M. **(L)** Psychometric curves in the  $T_{IN}$  condition are shown in the same format as **(D)** (same data as **K**). The monkey's saccade choice showed a bias away from the IVF in MDD task. **(M-O)** Chronometric curves for three conditions in the MDD task. **(P)** Chronometric curves in  $T_{IN}$  condition in the MDD task, for which trials were grouped based on target location.

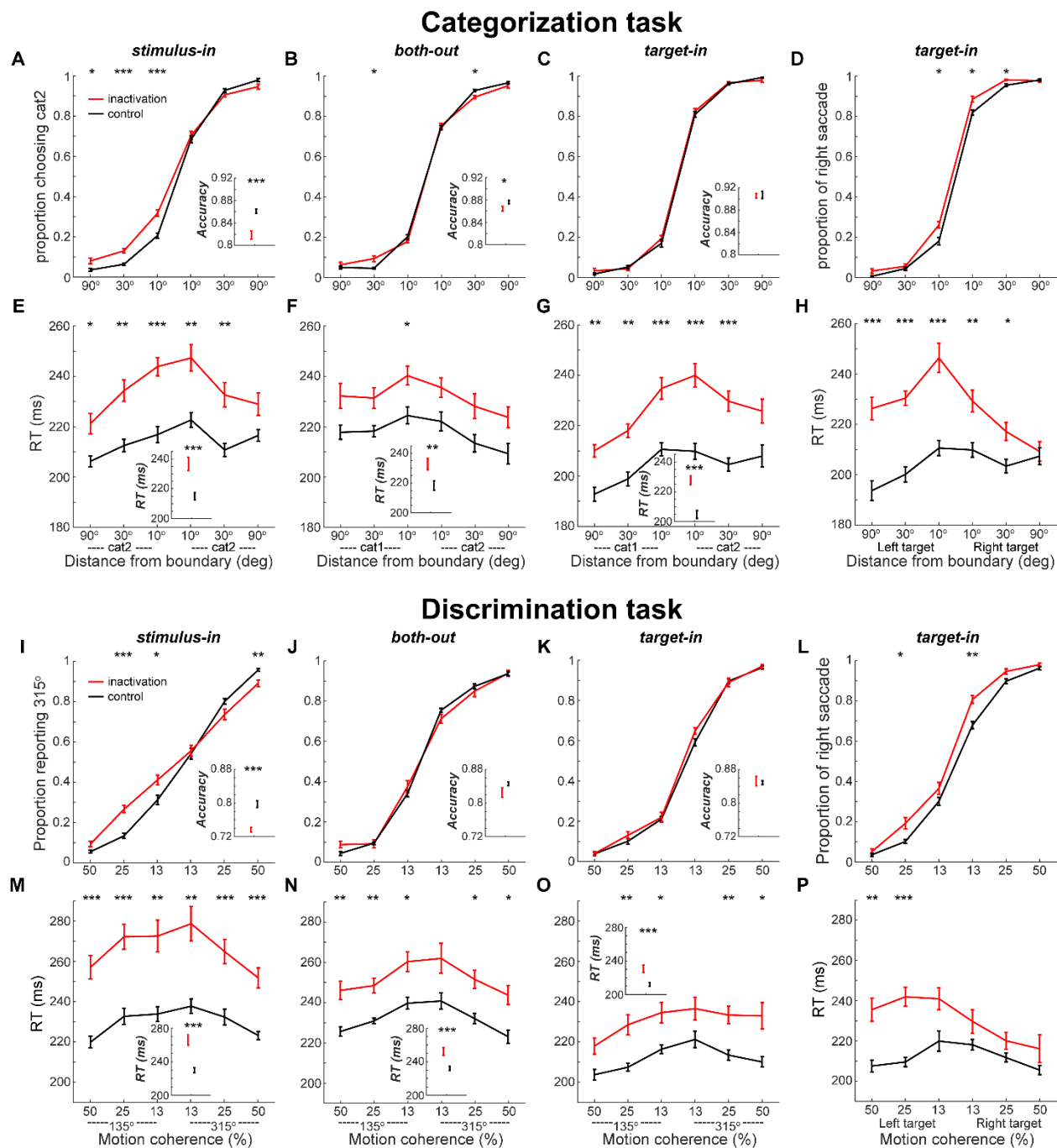
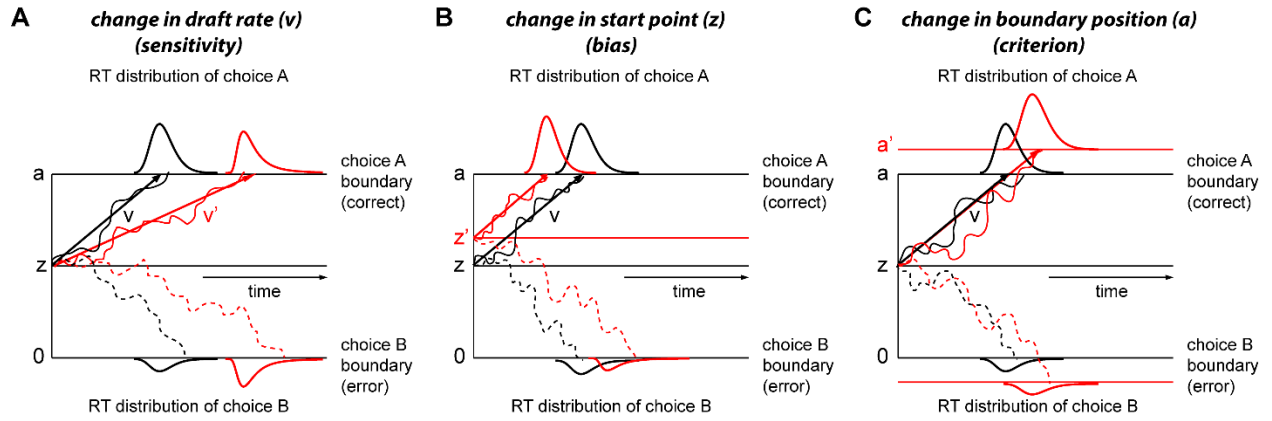


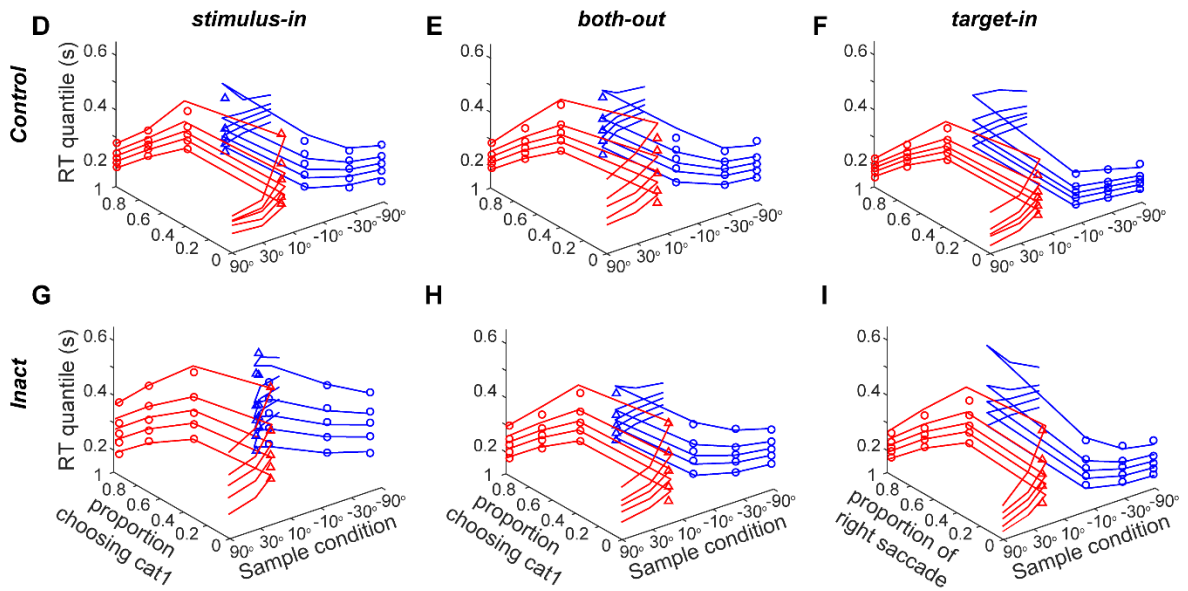
**Fig. S5.**

Behavioral performance of monkey B in inactivation and control sessions. Upper panels: Behavioral performance in MDC task. (A-C) Psychometric curves in  $S_{IN}$  (A),  $B_{OUT}$  (B) and  $T_{IN}$  (C) conditions in MDC task, shown separately for inactivation and control sessions. The choice accuracy was plotted as the proportion of choosing category 2 (red target). Trials from different saccade directions but the same difficulty level (angular distance from the boundary) were grouped for each category. Note that monkey B exhibited a larger decrease in accuracy for category 1 than category 2 in the  $S_{IN}$  condition. Therefore, category 1 was defined as the primary category for

monkey B. **(D)** Psychometric curves in  $T_{IN}$  conditions for which the trials were grouped based on the target location (same data as **C**). Choice accuracy is plotted as the proportion of rightward saccades. Trials of the same difficulty level from both categories were grouped for each target location. The monkey's saccade choice was biased away from the IVF (left visual field, the right hemisphere of monkey B was inactivated). **(E-G)** Chronometric curves for  $S_{IN}$  (**E**),  $B_{OUT}$  (**F**) and  $T_{IN}$  (**G**) conditions in the MDC task. **(H)** Chronometric curves in  $T_{IN}$  condition in MDC task, for which trials were grouped based on target location. The inset figure in each panel shows the global performance in each condition. The black stars indicate the statistical significance for the comparisons between control and inactivation sessions (\*:  $p < 0.05$ , \*\*:  $P < 0.01$ , \*\*\*:  $p < 0.001$ , unpaired t-test, multiple tests are Bonferroni corrected). The error bars denote  $\pm SEM$ . Lower panels: Behavioral performance in MDD task. **(I-K)** Psychometric curves in three conditions of the MDD task. The choice accuracy is plotted as the proportion of choosing  $315^\circ$  (red target, center direction of category 2). Trials from different saccade directions but same difficulty level (coherence) were grouped for each motion direction. Note that monkey B exhibited a larger decrease in accuracy for  $135^\circ$  than  $315^\circ$  stimuli in the  $S_{IN}$  conditions. Therefore,  $135^\circ$  was defined as the primary direction for monkey B. **(L)** Psychometric curves in the  $T_{IN}$  condition are shown in the same format as **(D)** (same data as **K**). The monkey's saccade choice showed a bias away from the IVF in MDD task. **(M-O)** Chronometric curves for three conditions in the MDD task. **(P)** Chronometric curves in  $T_{IN}$  condition in the MDD task, for which trials were grouped based on target location.



**MDC:**



**MDD:**

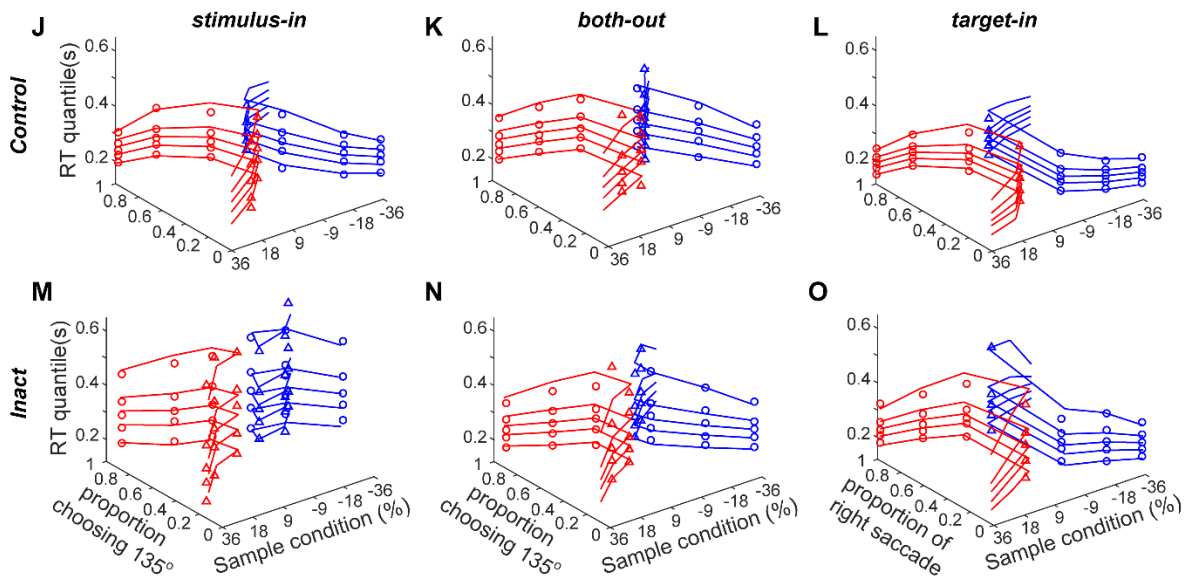
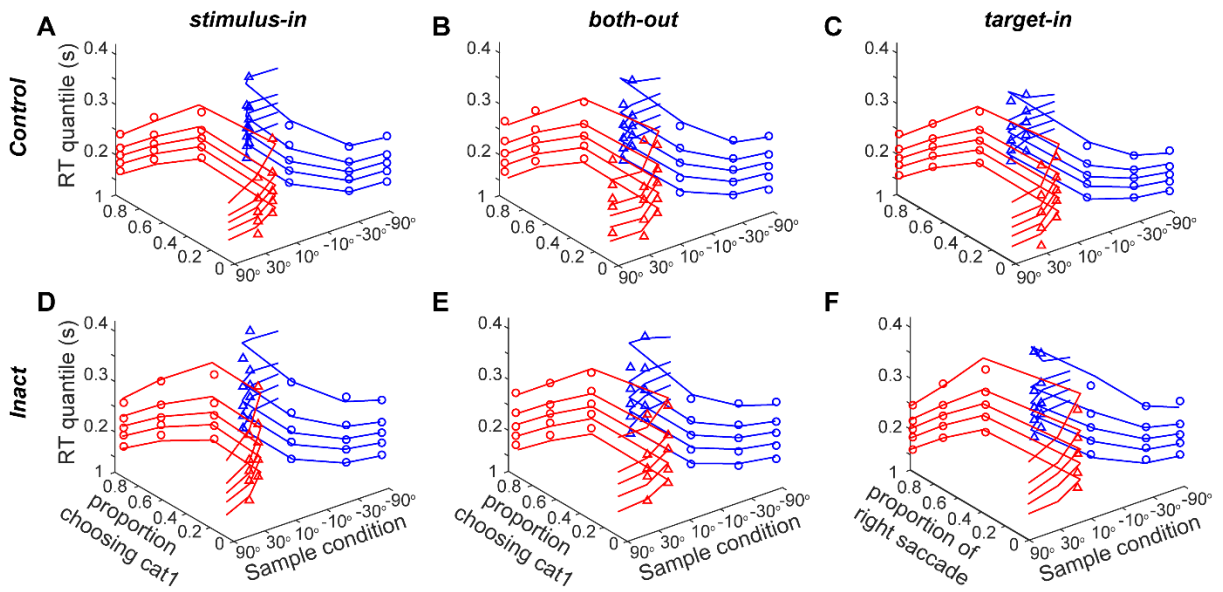


**Fig. S6.**

Drift diffusion model fits. **(A-C)**. Illustration of the drift diffusion model, and examples of how possible inactivation-induced variations in model parameters impact decision accuracy and reaction time. The drift diffusion model assumes that decisions are made by a noisy process that accumulates information over time from a starting point ( $z$ ) toward one of two choice boundaries ( $0$  and  $a$ ). A decision is made when one of the boundaries is reached. The rate of information accumulation is the drift rate ( $v$ ), and it is determined by the quality of the stimulus information. The sign of drift rate can be positive (mean drift rate toward the choice A boundary) or negative (mean drift rate toward the choice B boundary). Noise (within-trial variability) in the information accumulation process is present so that processes with the same mean drift rate do not always terminate at the same time (producing RT distributions) or the same boundary (producing errors). **(A)**. Effects of varying drift rate ( $v$ ) on accuracy and RT. The drift rate decreases from  $v$  (black) to  $v'$  (red). Only choice A trials are shown in this example, so that the diffusion process terminating at the choice A boundary is correct, while termination at the choice B boundary is incorrect. The slopes of colored arrows denote the mean drift rates in control (black) and inactivation (red) sessions. The curved solid and dashed traces depict fictive diffusion processes on single correct and incorrect trials, respectively, in control (black) and inactivation (red) conditions. The black and red right skewed gaussian distributions denote the RT distributions in control and inactivation sessions, respectively. A decrease in the drift rate results in lower accuracy as well as slower RT on both correct and error trials. Note the greater rightward skew in RT distributions during inactivation (red). **(B)**. Effects of varying start point ( $z$ ) on accuracy and RT. The start point of the diffusion process changes from  $z$  to  $z'$ , which is closer to the choice A boundary. This produces faster RTs on correct trials, slower RTs on error trials, as well as overall greater accuracy (i.e. increased probability of reaching the choice A boundary) **(C)**. Effects of varying the boundary position (i.e. height) ( $a$ ) on accuracy and RT. The boundary position increases from  $(0, a)$  to  $(0', a')$ , while the bias (the value of  $z$  relative to  $a/a'$ ) remains the same. This produces slower RTs on both correct and error trials, as well as greater accuracy. Note that changes in drift rate produces the greatest effect on both RT and accuracy. **(D-O)**. Drift diffusion model fits to monkey M's accuracy and RT data. Each panel is a quantile probability plot showing choice probabilities and RTs for both data and model fits across different stimulus conditions. Upper and lower panels show the results from the MDC and MDD tasks, respectively. Results from control and inactivation sessions are shown in different rows. Results from trials using the three different stimulus configurations are shown in different columns. For each panel, the stimulus conditions (MDC: the angular distance from motion directions within each category to the boundary; MDD: the coherence levels of each motion direction) are plotted on the x-axis, the probabilities of choosing category 1 (MDC task) or  $135^\circ$  (MDD task) for each stimulus condition are plotted on the y-axis, and the RT distribution percentiles (0.1, 0.3, 0.5, 0.7, 0.9) are plotted on the z-axis. Red and blue colors represent results for category 1/ $135^\circ$  and category 2/ $315^\circ$  trials, respectively, while the circles and triangles represent correct and error trials, respectively. Each colored trace shows a model fit. For error trials, only conditions in which there were sufficient numbers of trials ( $\geq 30$ ) are shown.

MDC:



MDD:

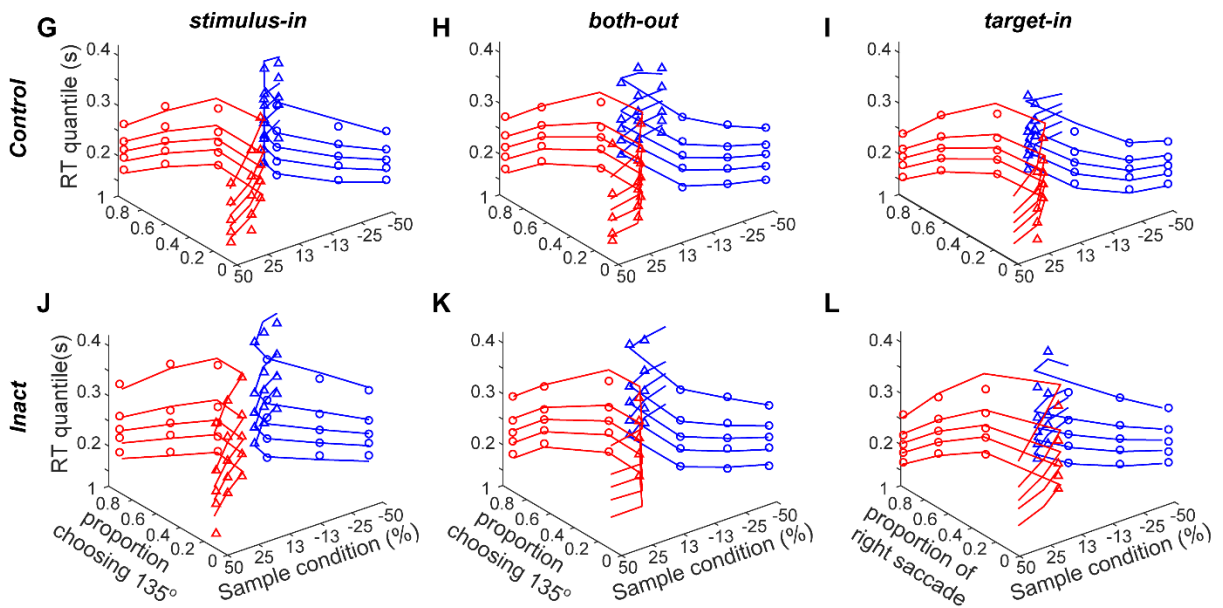


**Fig. S7.**

Drift diffusion model fits to monkey B's accuracy and RT data. The data and model fits in both MDC and MDD tasks are plotted in the same format as in **Fig S8**.

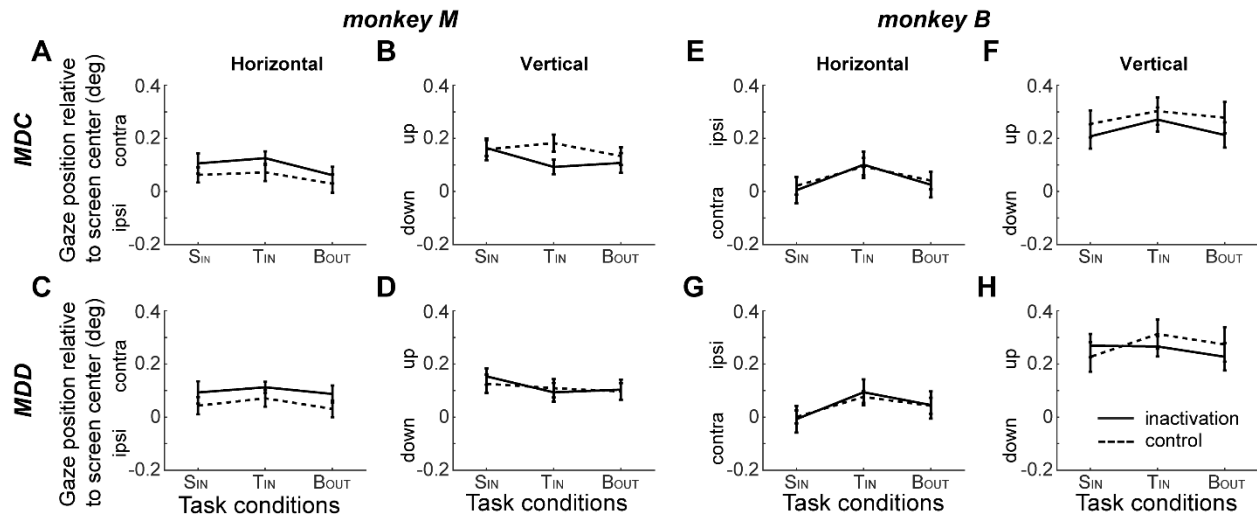
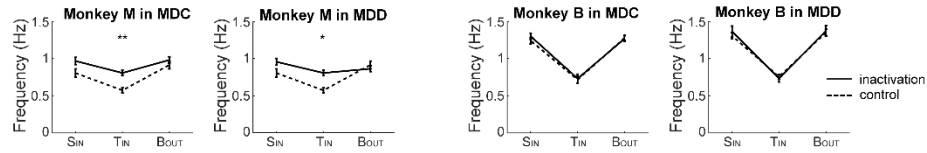


**Fig. S8.**

LIP inactivation did not influence the monkeys' gaze positions during the MDD and MDC tasks. This analysis tested whether LIP inactivation produced an obvious impairment of eye movements or profound spatial neglect. If there was a profound spatial neglect after LIP inactivation, monkeys' eye position during inactivation sessions would be expected shift away from the IVF, compared to control sessions. Only data from the time period following saccade target onset and before motion stimulus onset were included in this analysis. Left panels: data from monkey M. (A-B) The mean eye positions of monkey M in the three conditions of the MDC task were shown separately for horizontal (A) and vertical (B) directions. (C-D) The mean eye positions of monkey M in the three conditions of the MDD task, shown in the same format as (A) and (B). Right panels: data from monkey B. (E-F) The mean eye positions of monkey B in MDC task. (G-H) The mean eye positions of monkey B in MDD task. Note that there were no significant differences between control and inactivation sessions in all three conditions in both tasks.

Microsaccade frequency:



Microsaccade direction:

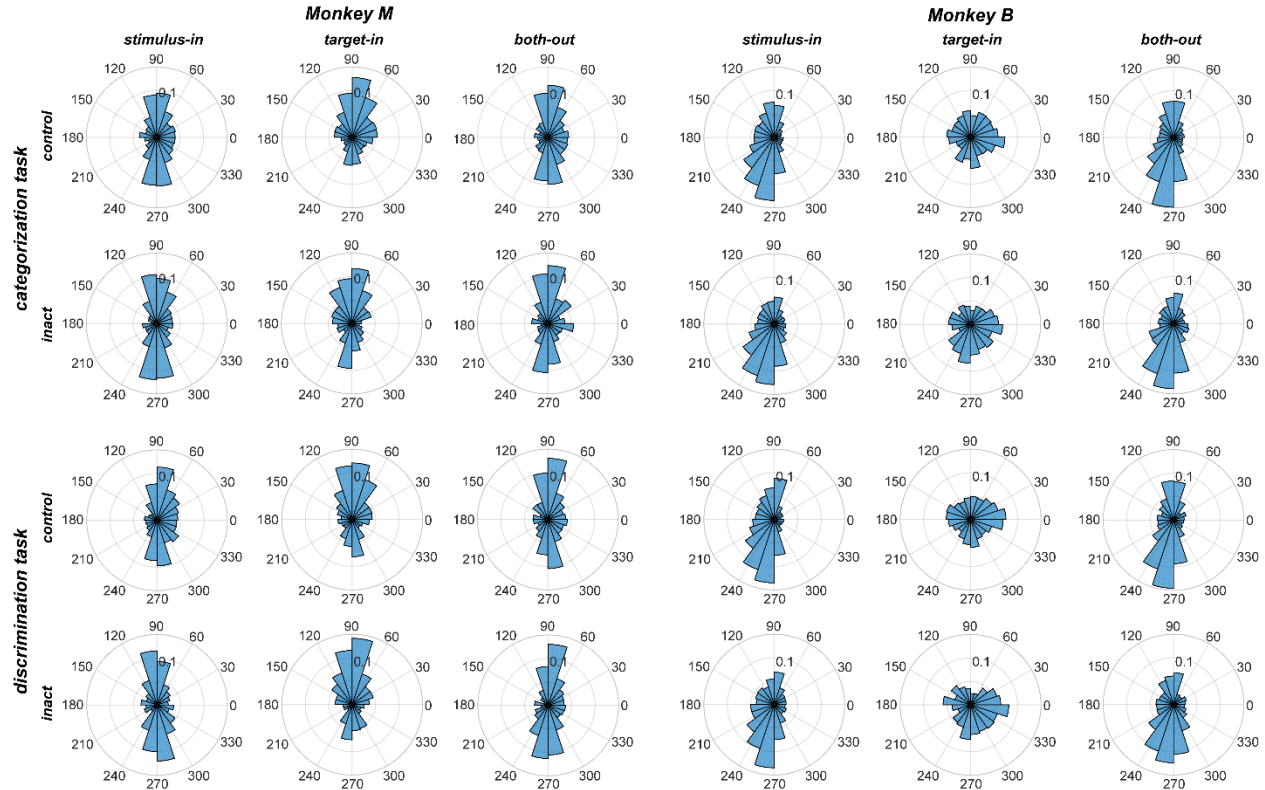


**Fig. S9.**

Frequency and direction of micro-saccades of each monkey during inactivation and control sessions. This analysis tested whether LIP inactivation produced an obvious impairment of eye movements. Only data from the time period following saccade target onset and before motion stimulus onset were included in this analysis. Upper panels: microsaccade frequency. Monkey M showed a trend for greater microsaccade frequency during both S<sub>IN</sub> and T<sub>IN</sub> conditions in both MDC and MDD following LIP inactivation. Monkey B did not show a difference in microsaccade frequency between inactivation and control sessions. Lower panels: the distributions of microsaccade direction. Data from the two monkeys are shown separately in the left and right panels. Note that the microsaccade direction for both monkeys in all three conditions of both tasks was not significantly biased away from the IVF (Monkey M: right; Monkey B, left). These results suggest that LIP inactivation did not produce an obvious impairment of eye movements.

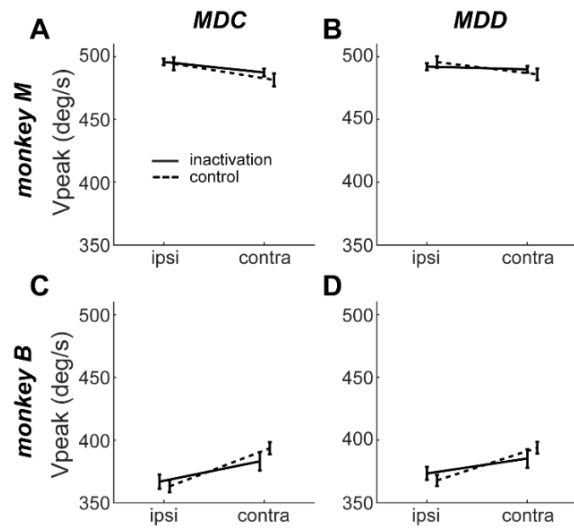


**Fig. S10.**

LIP inactivation did not influence the monkeys' peak saccade velocity during the MDD and MDC tasks. Only data from the  $T_{IN}$  condition in which one of the saccade targets was placed in the inactivated visual field were included in this analysis. (A) The mean peak saccade velocities of monkey M for both contralateral and ipsilateral saccades during the MDC task. (B) The mean peak saccade velocities of monkey M during MDD task. (C-D) The mean peak saccade velocities of monkey B during MDC (C) and MDD (D) tasks. Note that there were no significant differences between control and inactivation sessions for both contralateral and ipsilateral saccades in both tasks.

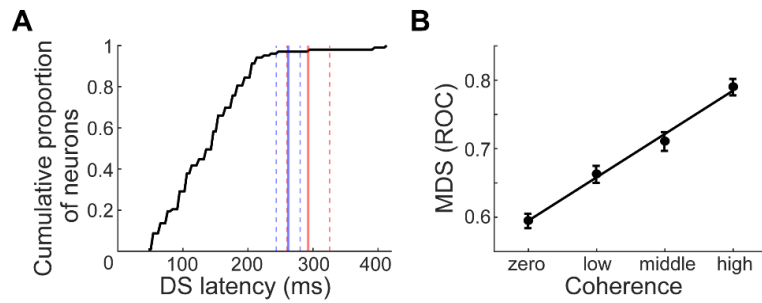


**Fig. S11.**

Motion direction selectivity of LIP neurons. **(A)** DS latency for LIP neurons. The red and blue solid lines indicate the mean RT of the two monkeys respectively, and the dashed colored lines indicate the corresponding  $\pm$ STD. Most DS neurons showed significant (one-way ANOVA,  $P < 0.01$ ) DS prior to the monkey's saccade choice. **(B)** Relationship between DS of LIP neurons and motion coherence. DS was quantified by ROC analysis using neuronal activity from 100-300 ms following motion stimuli onset. The error bar denotes  $\pm$ SEM, and the solid line indicates the linear fit.

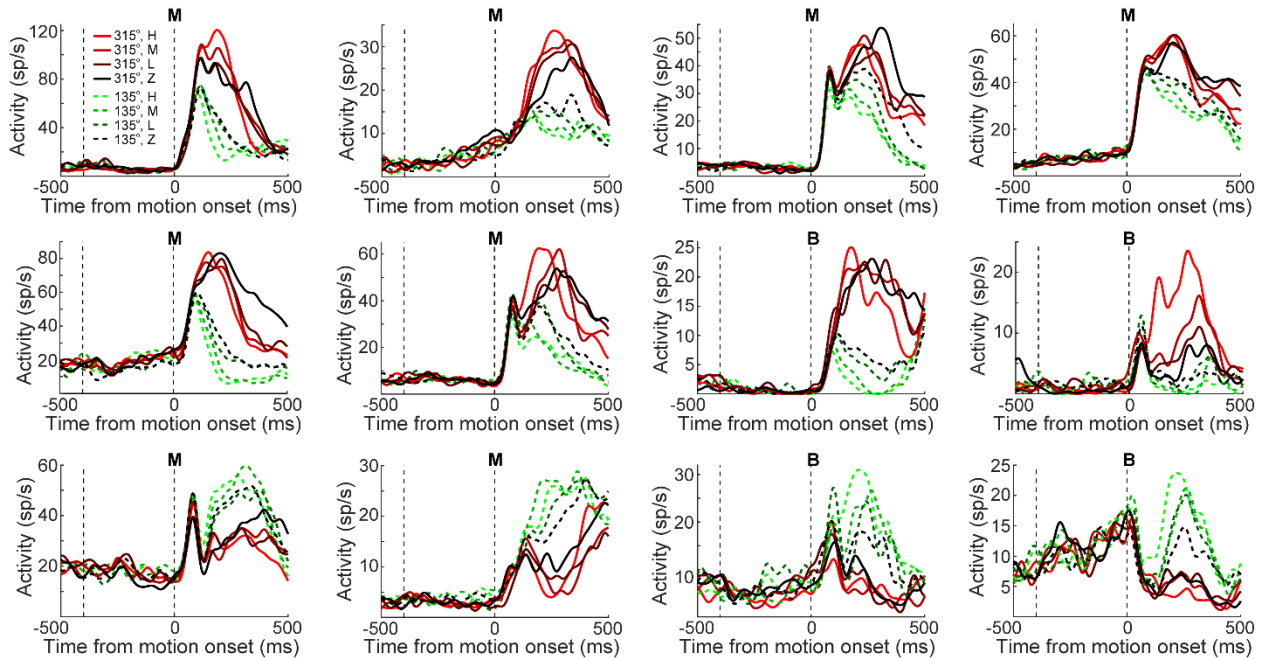


**Fig. S12.**

Example DS neurons recorded during the MDD task. Each panel shows neuronal activity for one example neuron. The motion stimulus but not the saccade targets appeared in neurons' RFs. The zero coherence trials were grouped according to the monkeys' choices about motion direction. Trials from both saccade directions were pooled for each coherence level. Only correct trials were used for non-zero coherence conditions. The two vertical dashed lines mark the time of target and motion stimulus onset, respectively. There are eight neurons shown for monkey M, while the other 4 neurons are from monkey B. Note that activity for each example neuron correlated with both the direction and coherence of motion. Note that on zero coherence trials (black traces), neuronal activity for each neuron correlated with the monkeys' decisions.

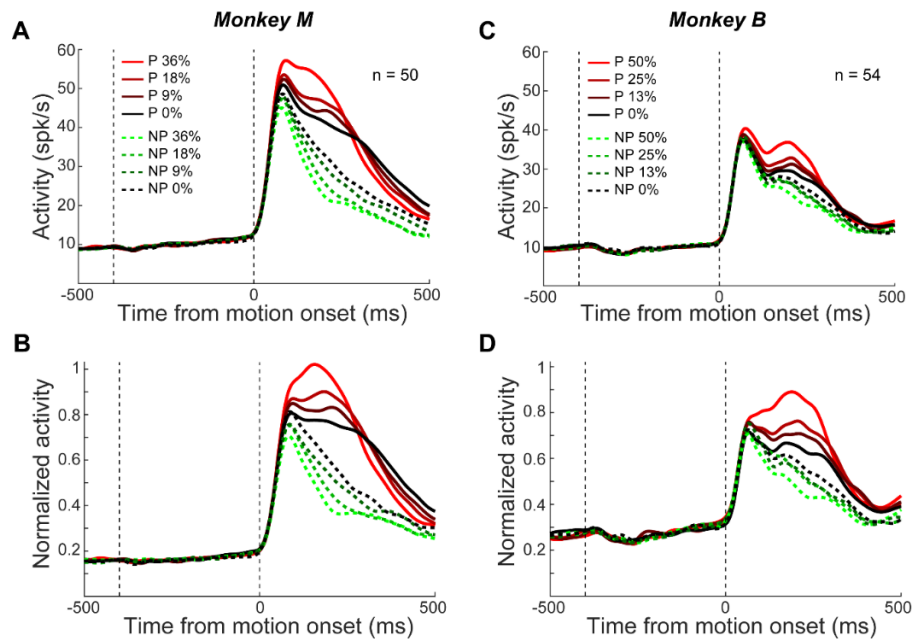


**Fig. S13.**

Population activity across DS neurons shown separately for each monkey. **(A)** Population activity of neurons from monkey M. Neuronal activity was pooled based on each neuron's preferred direction. The zero coherence trials were grouped according to the monkeys' choice. Only correct trials were used for non-zero coherence conditions. All neurons from monkey M were recorded by single channel electrode. **(B)** Normalized population activity of neurons recorded from monkey M. Activity of each neuron was normalized by its maximum activity. **(C-D)** Population activity recorded from monkey B, which was primarily recorded by a 16 channel linear array.

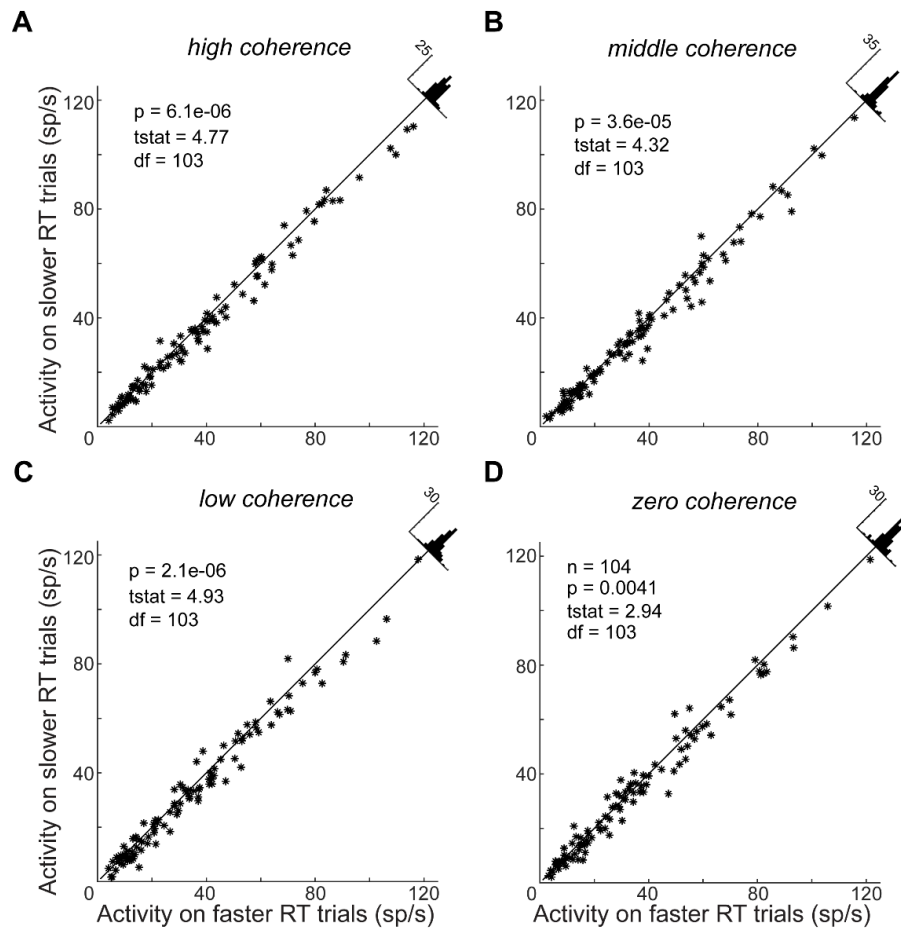


**Fig. S14.**

Comparison of LIP activity between faster and slower RT trials. **(A)** LIP neurons' response (mean firing rate) to high coherence motion stimuli within the faster (x-axis) RT and slower RT (y-axis) trial groups. Each dot denotes a single neuron's response to its preferred motion direction. Neuronal activity within a 200 ms window starting at motion stimulus onset on correct trials was used in the analysis. The inset histogram shows the distribution of differential activity between faster and slower RT trial groups. **(B-D)** LIP neurons' response to middle **(B)**, low **(C)** and zero **(D)** coherence motion stimuli within the faster and slower RT trial groups.

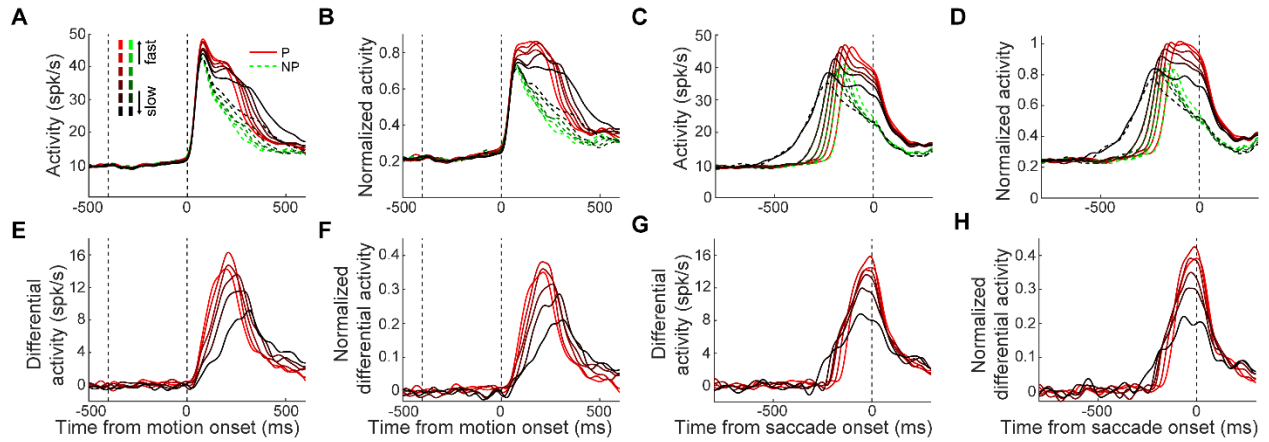


**Fig. S15.**

LIP neurons' response to motion stimuli correlated with monkeys' RTs. **(A)** Population activity of DS selective neurons grouped in six RT bins. Neuronal activity was pooled based on each neuron's preferred direction. The zero coherence trials were grouped according to the monkeys' choices about motion direction. Trials from both saccade directions were pooled for each coherence level. Only correct trials were used for non-zero coherence conditions. The red and green colors denote neural activity in preferred and non-preferred direction, respectively. Different colors indicate the RT values from low to high. **(B)** Normalized population activity of DS selective LIP neurons grouped in six RT bins. **(C-D)** Population activity of DS selective LIP neurons aligned to saccade onset. LIP neurons' response to motion stimuli did not converge to a common threshold. **(E-H)** Population differential activity of DS selective LIP neurons aligned to either stimulus onset (**E-F**) or saccade onset (**G-H**). Note that the slope of differential activity correlated with monkeys' RTs.

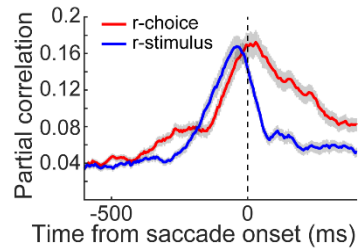


**Fig. S16.**

Partial correlation analysis. The value of  $r$ -stimulus (partial correlation between neuronal activity and stimulus direction, given the monkeys' choices) and  $r$ -choice (partial correlation between neuronal activity and monkeys' choice, given the stimulus direction) are plotted separately across time. Shaded areas denote  $\pm$ SEM.  $r$ -stimulus decreases around the time of the monkey's choice (saccade), while  $r$ -choice persists beyond the time of the monkey's choice.

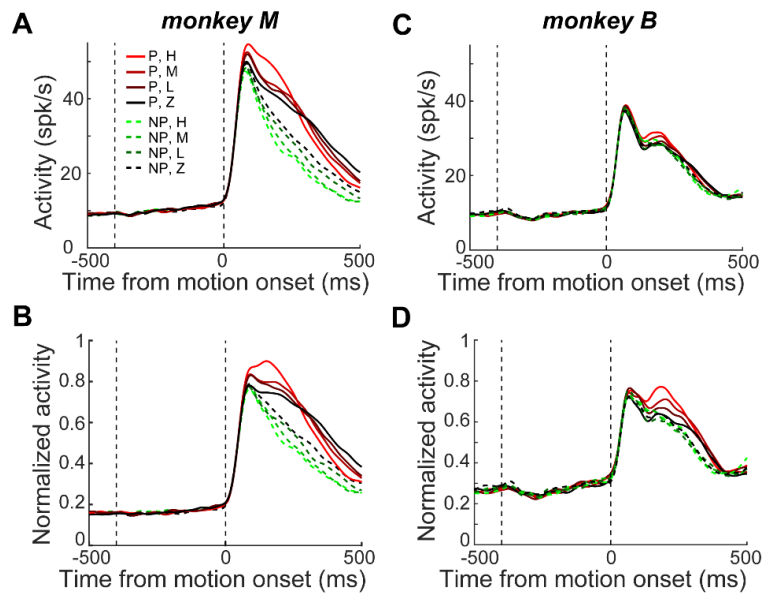


**Fig. S17.**

Relationship between activity of DS neurons and behavioral impact of inactivating individual LIP sites. **(A)** Population activity of all DS neurons from Monkey M. Activity was pooled based on the primary direction (P,  $315^\circ$ ), for which behavior was more greatly impacted on average across all sessions. At the population level, LIP neurons' response to the primary direction ( $315^\circ$ ) was significantly greater than that to non-primary direction (NP,  $135^\circ$ ). **(B)** The same as **(A)**, but with normalized population activity. **(C-D)** Population activity of all DS neurons recorded from Monkey B. Neural activity was pooled according to each site's preference revealed by the pattern of behavioral deficits observed during inactivation (see Methods).

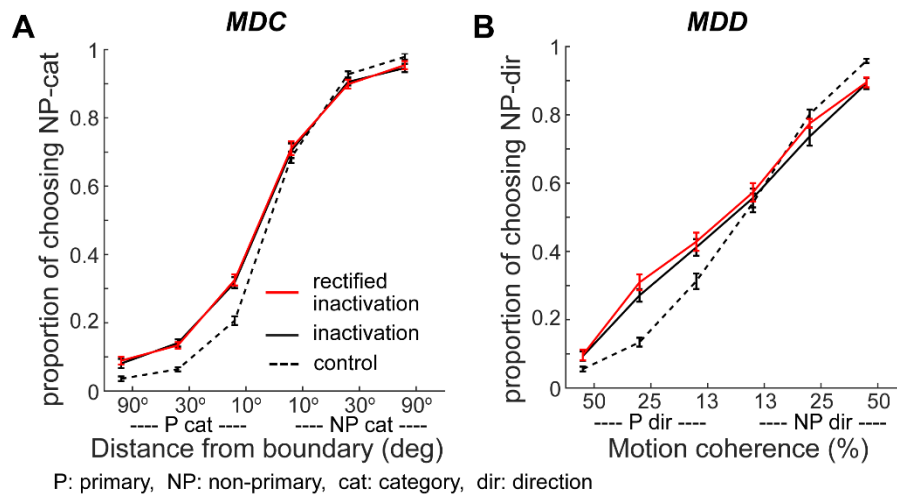


**Fig. S18.**

Behavioral performance of Monkey B in the  $S_{IN}$  condition of both MDC and MDD tasks. The primary (P) and non-primary (NP) categories/directions were computed according to the preferences of neurons at each recording/inactivation site (see Methods). (A) Monkey B's MDC task performance. The red trace shows performance on inactivation sessions when defining the primary category/direction according to the stimulus preference of neurons at each inactivation site. The black trace shows the same data with the primary category/direction defined globally according to the behavioral impact on performance on average across all inactivation sessions (as in Fig 2). Note the similar pattern of results for each method of defining the primary category. (B) Monkey B's MDD task performance. Note the similar results (and a non-significant trend toward a greater effect) when defining the primary direction by taking into account each site's stimulus preference (red), compared to the global method (black).

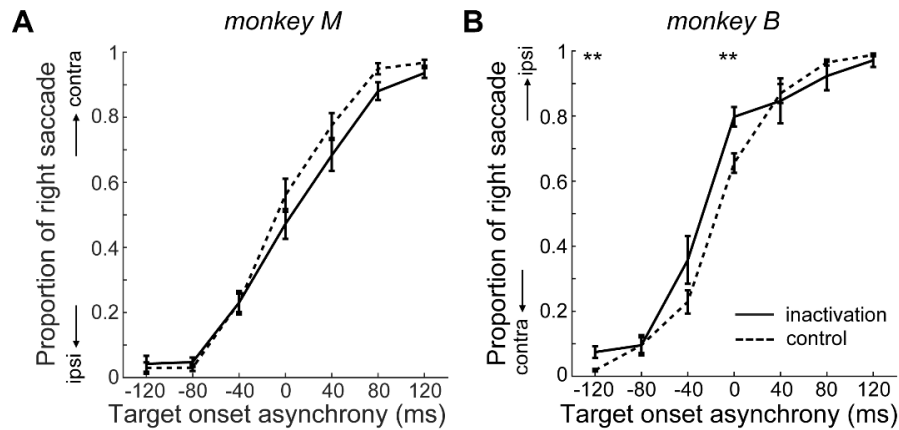


**Fig. S19.**

Behavioral performance in the free choice task in control and inactivation sessions. Data from each monkey is shown separately. Choice accuracy is plotted as the proportion of right saccades for each target onset asynchrony condition (left target onset time relative to right target onset time). The left and right hemispheres were inactivated for monkeys M and B, respectively. Therefore, the IVFs (contralateral) are right and left visual field for monkeys M and B, respectively. Note that both monkeys' saccade choices in the inactivation sessions were biased away from the inactivated visual field, compared to control sessions. The black stars indicate the statistical significance for comparisons between control and inactivation sessions (\*\*:  $P < 0.01$ , unpaired t-test, Bonferroni corrected).

## Supplementary Tables:

**Table. S1-S4:** Results of fitting drift diffusion models with fixed boundaries. We bootstrapped the drift diffusion model fitting 1000 times for each task condition. The tables show the fitted values and standard deviations of the resulting parameters for the 1000 non-parametric bootstrap iterations. The red color marks the parameters for which there were significant differences between inactivation and control sessions ( $p < 0.05$ , bootstrap). Results from different monkeys in different tasks are shown separately in different tables. We call attention to two results in the tables below. First, for both monkeys, only drift rates ( $v$ ) in  $S_{IN}$  conditions in both tasks significantly decreased in inactivation sessions compared to control sessions. Second, the start point of the diffusion process (bias,  $z/a$ ) and the decision boundary ( $a$ ) in  $T_{IN}$  conditions significantly changed across tasks and monkeys.  $R^2$ : the proportion of the explained variance.

**Table. S1.**

Parameters for the diffusion model fits to Monkey M's behavioral data in MDC task.

Task conditions		Fitted parameters							Stats		
		A	$T_{er}$	$s_t$	Z, Z/a	$s_z$	$\eta$	v	AICc	BIC	R <sup>2</sup>
S <sub>IN</sub>	control	0.087±0.004	0.202±0.003	0.200±0.046	0.048±0.002 , 0.550±0.027	0.062±0.009	0.096±0.005	1.289±0.101, 1.031±0.075, 0.469±0.058, -0.419±0.045, -0.687±0.061, -0.854±0.084	10910	10981	0.966
	inact	0.082±0.003	0.228±0.009	0.145±0.042	0.050±0.002 , 0.611±0.028	0.046±0.009	0.181±0.019	0.599±0.070, 0.415±0.054, 0.201±0.042, -0.123±0.027, -0.308±0.037, -0.456±0.054	9604	9672	0.930
B <sub>OUT</sub>	control	0.080±0.002	0.199±0.003	0.156±0.027	0.051±0.002 , 0.637±0.026	0.012±0.010	0.098±0.007	0.790±0.045, 0.499±0.034, 0.287±0.027, -0.344±0.029, -0.617±0.036, -0.740±0.047	12065	12137	0.916
	inact	0.080±0.004	0.193±0.004	0.124±0.048	0.045±0.002 , 0.569±0.028	0.048±0.010	0.106±0.008	0.758±0.079, 0.556±0.061, 0.303±0.048, -0.350±0.030, -0.524±0.041, -0.645±0.059	7592	7658	0.968
T <sub>IN</sub>	control	0.070±0.003	0.161±0.002	0.243±0.048	0.035±0.002 , 0.496±0.023	0.025±0.014	0.068±0.003	1.259±0.113, 0.880±0.085, 0.475±0.066, -0.544±0.040, -0.684±0.058, -0.887±0.085	11275	11346	0.965
	inact	0.086±0.008	0.177±0.004	0.237±0.076	0.036±0.003 , 0.425±0.034	0.052±0.018	0.105±0.007	1.147±0.179, 0.745±0.127, 0.408±0.090, -0.449±0.096, -0.731±0.133, -0.897±0.185	7187	7253	0.932

**Table. S2.**

Parameters for the diffusion model fits to Monkey M's behavioral data in MDD task.

Task conditions		Fitted parameters							Stats		
		A	$T_{er}$	$s_t$	$z, z/a$	$s_z$	$\eta$	$v$	AICc	BIC	$R^2$
S <sub>IN</sub>	control	0.068±0.002	0.223±0.003	0.160±0.035	0.045±0.002 , 0.664±0.031	0.011±0.010	0.130±0.007	0.750±0.048, 0.283±0.037, 0.053±0.029, -0.251±0.033, -0.545±0.041, -0.948±0.053	8151	8218	0.937
	inact	0.093±0.004	0.252±0.008	0.229±0.053	0.051±0.002 , 0.552±0.025	0.078±0.011	0.214±0.014	0.381±0.043, 0.128±0.034, 0.058±0.029, -0.012±0.017, -0.049±0.021, -0.258±0.028	8423	8488	0.957
B <sub>O</sub> UT	control	0.069±0.003	0.231±0.005	0.176±0.046	0.042±0.002 , 0.612±0.029	0.028±0.011	0.145±0.009	0.448±0.062, 0.258±0.048, 0.143±0.039, -0.046±0.024, -0.264±0.032, -0.682±0.044	8666	8733	0.939
	inact	0.085±0.006	0.214±0.008	0.282±0.081	0.045±0.002 , 0.533±0.029	0.069±0.016	0.135±0.011	0.563±0.125, 0.264±0.095, 0.134±0.074, -0.102±0.039, -0.335±0.058, -0.648±0.087	6856	6920	0.982
T <sub>IN</sub>	control	0.062±0.003	0.170±0.002	0.198±0.043	0.038±0.002 , 0.614±0.003	0.012±0.010	0.091±0.004	0.798±0.077, 0.465±0.060, 0.129±0.048, -0.409±0.042, -0.620±0.052, -0.862±0.088	8113	8180	0.961
	inact	0.090±0.011	0.189±0.006	0.330±0.104	0.046±0.005 , 0.512±0.056	0.068±0.019	0.118±0.009	0.898±0.197, 0.528±0.141, 0.320±0.101, -0.425±0.104, -0.594±0.143, -1.054±0.199	4729	4789	0.966

**Table. S3.**

Parameters for the diffusion model fits to Monkey B's behavioral data in MDC task.

Task conditions		Fitted parameters							Stats		
		a	T <sub>er</sub>	s <sub>t</sub>	z, z/a	s <sub>z</sub>	η	v	AICc	BIC	R <sup>2</sup>
S <sub>IN</sub>	control	0.060±0.003	0.179±0.002	0.362±0.070	0.028±0.001 , 0.474±0.024	0.048±0.005	0.074±0.003	1.075±0.126., 0.888±0.098, 0.554±0.071, -0.233±0.038, -0.799±0.095, -0.872±0.106	28387	28469	0.916
	inact	0.062±0.003	0.180±0.003	0.190±0.069	0.029±0.001 , 0.473±0.024	0.039±0.008	0.080±0.004	0.684±0.107, 0.479±0.078, 0.222±0.048, -0.178±0.033, -0.453±0.070, -0.563±0.089	16628	16703	0.954
B <sub>OUT</sub>	control	0.059±0.002	0.178±0.002	0.294±0.060	0.030±0.001 , 0.503±0.023	0.044±0.006	0.096±0.003	0.754±0.072, 0.772±0.069, 0.439±0.042, -0.343±0.036, -0.760±0.066, -0.892±0.075	29651	29734	0.956
	inact	0.062±0.005	0.188±0.003	0.377±0.095	0.031±0.003 , 0.504±0.042	0.049±0.010	0.100±0.005	0.800±0.171, 0.733±0.116, 0.500±0.085, -0.407±0.073, -0.717±0.114, -0.917±0.149.	14798	14871	0.964
T <sub>IN</sub>	control	0.057±0.003	0.168±0.001	0.254±0.062	0.029±0.002 , 0.508±0.031	0.041±0.006	0.077±0.002	0.925±0.126, 0.801±0.098, 0.447±0.062, -0.480±0.065, -0.863±0.100, -1.136±0.143	25731	25811	0.977
	inact	0.066±0.004	0.172±0.002	0.157±0.066	0.039±0.002 , 0.588±0.033	0.032±0.009	0.083±0.004	0.850±0.186, 0.666±0.105, 0.362±0.066, -0.307±0.043, -0.697±0.082, -0.883±0.081	13200	13273	0.955

**Table. S4.**

Parameters for the diffusion model fits to Monkey B's behavioral data in MDD task.

Task conditions		Fitted parameters							Stats		
		a	$T_{er}$	$s_t$	z, z/a	$s_z$	$\eta$	v	AICc	BIC	$R^2$
$S_{IN}$	control	0.058±0.002	0.184±0.002	0.280±0.061	0.027±0.001 , 0.460±0.021	0.036±0.006	0.087±0.004	0.829±0.094, 0.525±0.064, 0.267±0.044, -0.023±0.029, -0.372±0.053, -0.711±0.100	18958	19034	0.929
	inact	0.068±0.005	0.188±0.005	0.200±0.101	0.031±0.003 , 0.461±0.037	0.035±0.012	0.093±0.007	0.481±0.123, 0.251±0.066, 0.123±0.045, -0.016±0.031, -0.196±0.065, -0.403±0.112	12268	12339	0.972
$B_{OUT}$	control	0.059±0.004	0.190±0.002	0.303±0.085	0.031±0.002 , 0.517±0.032	0.048±0.008	0.102±0.003	0.806±0.128, 0.666±0.102, 0.195±0.047, -0.383±0.066, -0.634±0.090, -0.886±0.117	19657	19734	0.938
	inact	0.061±0.003	0.195±0.004	0.241±0.075	0.030±0.002 , 0.489±0.033	0.033±0.011	0.102±0.006	0.569±0.105, 0.567±0.109, 0.141±0.045, -0.246±0.049, -0.403±0.077, -0.613±0.110	10050	10118	0.978
$T_{IN}$	control	0.055±0.002	0.166±0.002	0.145±0.067	0.031±0.001 , 0.561±0.025	0.033±0.005	0.084±0.004	0.693±0.108, 0.452±0.068, 0.143±0.044, -0.288±0.042, -0.609±0.079, -0.780±0.085	19766	19844	0.988
	inact	0.066±0.003	0.174±0.003	0.226±0.055	0.041±0.002 , 0.626±0.026	0.034±0.006	0.083±0.006	0.772±0.140, 0.489±0.075, 0.238±0.049, -0.265±0.039, -0.469±0.066, -0.733±0.063	10110	10180	0.917

## References and Notes

1. R. A. Andersen, Visual and eye movement functions of the posterior parietal cortex. *Annu. Rev. Neurosci.* **12**, 377–403 (1989). [doi:10.1146/annurev.ne.12.030189.002113](https://doi.org/10.1146/annurev.ne.12.030189.002113) [Medline](#)
2. G. J. Blatt, R. A. Andersen, G. R. Stoner, Visual receptive field organization and cortico-cortical connections of the lateral intraparietal area (area LIP) in the macaque. *J. Comp. Neurol.* **299**, 421–445 (1990). [doi:10.1002/cne.902990404](https://doi.org/10.1002/cne.902990404) [Medline](#)
3. J. W. Lewis, D. C. Van Essen, Corticocortical connections of visual, sensorimotor, and multimodal processing areas in the parietal lobe of the macaque monkey. *J. Comp. Neurol.* **428**, 112–137 (2000). [doi:10.1002/1096-9861\(20001204\)428:1<112::AID-CNE8>3.0.CO;2-9](https://doi.org/10.1002/1096-9861(20001204)428:1<112::AID-CNE8>3.0.CO;2-9) [Medline](#)
4. E. P. Cook, J. H. Maunsell, Dynamics of neuronal responses in macaque MT and VIP during motion detection. *Nat. Neurosci.* **5**, 985–994 (2002). [doi:10.1038/nn924](https://doi.org/10.1038/nn924) [Medline](#)
5. V. de Lafuente, M. Jazayeri, M. N. Shadlen, Representation of accumulating evidence for a decision in two parietal areas. *J. Neurosci.* **35**, 4306–4318 (2015). [doi:10.1523/JNEUROSCI.2451-14.2015](https://doi.org/10.1523/JNEUROSCI.2451-14.2015) [Medline](#)
6. D. J. Freedman, J. A. Assad, Experience-dependent representation of visual categories in parietal cortex. *Nature* **443**, 85–88 (2006). [doi:10.1038/nature05078](https://doi.org/10.1038/nature05078) [Medline](#)
7. J. D. Roitman, M. N. Shadlen, Response of neurons in the lateral intraparietal area during a combined visual discrimination reaction time task. *J. Neurosci.* **22**, 9475–9489 (2002). [doi:10.1523/JNEUROSCI.22-21-09475.2002](https://doi.org/10.1523/JNEUROSCI.22-21-09475.2002) [Medline](#)
8. M. N. Shadlen, W. T. Newsome, Motion perception: Seeing and deciding. *Proc. Natl. Acad. Sci. U.S.A.* **93**, 628–633 (1996). [doi:10.1073/pnas.93.2.628](https://doi.org/10.1073/pnas.93.2.628) [Medline](#)
9. S. K. Swaminathan, D. J. Freedman, Preferential encoding of visual categories in parietal cortex compared with prefrontal cortex. *Nat. Neurosci.* **15**, 315–320 (2012). [doi:10.1038/nn.3016](https://doi.org/10.1038/nn.3016) [Medline](#)
10. S. K. Swaminathan, N. Y. Masse, D. J. Freedman, A comparison of lateral and medial intraparietal areas during a visual categorization task. *J. Neurosci.* **33**, 13157–13170 (2013). [doi:10.1523/JNEUROSCI.5723-12.2013](https://doi.org/10.1523/JNEUROSCI.5723-12.2013) [Medline](#)
11. Z. M. Williams, J. C. Elfar, E. N. Eskandar, L. J. Toth, J. A. Assad, Parietal activity and the perceived direction of ambiguous apparent motion. *Nat. Neurosci.* **6**, 616–623 (2003). [doi:10.1038/nn1055](https://doi.org/10.1038/nn1055) [Medline](#)
12. M. N. Shadlen, W. T. Newsome, Neural basis of a perceptual decision in the parietal cortex (area LIP) of the rhesus monkey. *J. Neurophysiol.* **86**, 1916–1936 (2001). [doi:10.1152/jn.2001.86.4.1916](https://doi.org/10.1152/jn.2001.86.4.1916) [Medline](#)
13. D. J. Freedman, J. A. Assad, Neuronal Mechanisms of Visual Categorization: An Abstract View on Decision Making. *Annu. Rev. Neurosci.* **39**, 129–147 (2016). [doi:10.1146/annurev-neuro-071714-033919](https://doi.org/10.1146/annurev-neuro-071714-033919) [Medline](#)
14. J. I. Gold, M. N. Shadlen, The neural basis of decision making. *Annu. Rev. Neurosci.* **30**, 535–574 (2007). [doi:10.1146/annurev.neuro.29.051605.113038](https://doi.org/10.1146/annurev.neuro.29.051605.113038) [Medline](#)

15. A. C. Huk, L. N. Katz, J. L. Yates, The Role of the Lateral Intraparietal Area in (the Study of) Decision Making. *Annu. Rev. Neurosci.* **40**, 349–372 (2017). [doi:10.1146/annurev-neuro-072116-031508](https://doi.org/10.1146/annurev-neuro-072116-031508) [Medline](#)
16. L. N. Katz, J. L. Yates, J. W. Pillow, A. C. Huk, Dissociated functional significance of decision-related activity in the primate dorsal stream. *Nature* **535**, 285–288 (2016). [doi:10.1038/nature18617](https://doi.org/10.1038/nature18617) [Medline](#)
17. T. D. Hanks, J. Ditterich, M. N. Shadlen, Microstimulation of macaque area LIP affects decision-making in a motion discrimination task. *Nat. Neurosci.* **9**, 682–689 (2006). [doi:10.1038/nn1683](https://doi.org/10.1038/nn1683) [Medline](#)
18. S. Shushruth, M. Mazurek, M. N. Shadlen, Comparison of Decision-Related Signals in Sensory and Motor Preparatory Responses of Neurons in Area LIP. *J. Neurosci.* **38**, 6350–6365 (2018). [doi:10.1523/JNEUROSCI.0668-18.2018](https://doi.org/10.1523/JNEUROSCI.0668-18.2018) [Medline](#)
19. A. Zaidel, G. C. DeAngelis, D. E. Angelaki, Decoupled choice-driven and stimulus-related activity in parietal neurons may be misrepresented by choice probabilities. *Nat. Commun.* **8**, 715 (2017). [doi:10.1038/s41467-017-00766-3](https://doi.org/10.1038/s41467-017-00766-3) [Medline](#)
20. G. Ibos, D. J. Freedman, Sequential sensory and decision processing in posterior parietal cortex. *eLife* **6**, e23743 (2017). [doi:10.7554/eLife.23743](https://doi.org/10.7554/eLife.23743) [Medline](#)
21. J. W. Bisley, M. E. Goldberg, Attention, intention, and priority in the parietal lobe. *Annu. Rev. Neurosci.* **33**, 1–21 (2010). [doi:10.1146/annurev-neuro-060909-152823](https://doi.org/10.1146/annurev-neuro-060909-152823) [Medline](#)
22. C. L. Colby, M. E. Goldberg, Space and attention in parietal cortex. *Annu. Rev. Neurosci.* **22**, 319–349 (1999). [doi:10.1146/annurev.neuro.22.1.319](https://doi.org/10.1146/annurev.neuro.22.1.319) [Medline](#)
23. C. Wardak, E. Olivier, J. R. Duhamel, A deficit in covert attention after parietal cortex inactivation in the monkey. *Neuron* **42**, 501–508 (2004). [doi:10.1016/S0896-6273\(04\)00185-0](https://doi.org/10.1016/S0896-6273(04)00185-0) [Medline](#)
24. R. A. Andersen, C. A. Buneo, Intentional maps in posterior parietal cortex. *Annu. Rev. Neurosci.* **25**, 189–220 (2002). [doi:10.1146/annurev.neuro.25.112701.142922](https://doi.org/10.1146/annurev.neuro.25.112701.142922) [Medline](#)
25. Y. Liu, E. A. Yttri, L. H. Snyder, Intention and attention: Different functional roles for LIPd and LIPv. *Nat. Neurosci.* **13**, 495–500 (2010). [doi:10.1038/nn.2496](https://doi.org/10.1038/nn.2496) [Medline](#)
26. X. Yu, Y. Gu, Probing sensory readout via combined choice-correlation measures and microstimulation perturbation. *Neuron* **100**, 715–727.e5 (2018). [doi:10.1016/j.neuron.2018.08.034](https://doi.org/10.1016/j.neuron.2018.08.034) [Medline](#)
27. J. K. Fitzgerald, D. J. Freedman, A. Fanini, S. Bennur, J. I. Gold, J. A. Assad, Biased associative representations in parietal cortex. *Neuron* **77**, 180–191 (2013). [doi:10.1016/j.neuron.2012.11.014](https://doi.org/10.1016/j.neuron.2012.11.014) [Medline](#)
28. P. F. Balan, J. Gottlieb, Functional significance of nonspatial information in monkey lateral intraparietal area. *J. Neurosci.* **29**, 8166–8176 (2009). [doi:10.1523/JNEUROSCI.0243-09.2009](https://doi.org/10.1523/JNEUROSCI.0243-09.2009) [Medline](#)
29. M. N. Shadlen, R. Kiani, T. D. Hanks, A. K. Churchland, “Neurobiology of decision making: An intentional framework” in *Better than Conscious? Decision Making, the Human*

- Mind, and Implications for Institutions*, C. Engel, W. Singer, Eds. (MIT Press, 2008), pp. 71–101.
30. J. L. Yates, I. M. Park, L. N. Katz, J. W. Pillow, A. C. Huk, Functional dissection of signal and noise in MT and LIP during decision-making. *Nat. Neurosci.* **20**, 1285–1292 (2017). [doi:10.1038/nn.4611](https://doi.org/10.1038/nn.4611) [Medline](#)
  31. T. B. Crapse, H. Lau, M. A. Basso, A role for the superior colliculus in decision criteria. *Neuron* **97**, 181–194.e6 (2018). [doi:10.1016/j.neuron.2017.12.006](https://doi.org/10.1016/j.neuron.2017.12.006) [Medline](#)
  32. C. A. Seger, E. K. Miller, Category learning in the brain. *Annu. Rev. Neurosci.* **33**, 203–219 (2010). [doi:10.1146/annurev.neuro.051508.135546](https://doi.org/10.1146/annurev.neuro.051508.135546) [Medline](#)
  33. A. M. Licata, M. T. Kaufman, D. Raposo, M. B. Ryan, J. P. Sheppard, A. K. Churchland, Posterior Parietal Cortex Guides Visual Decisions in Rats. *J. Neurosci.* **37**, 4954–4966 (2017). [doi:10.1523/JNEUROSCI.0105-17.2017](https://doi.org/10.1523/JNEUROSCI.0105-17.2017) [Medline](#)
  34. T. D. Hanks, C. D. Kopec, B. W. Brunton, C. A. Duan, J. C. Erlich, C. D. Brody, Distinct relationships of parietal and prefrontal cortices to evidence accumulation. *Nature* **520**, 220–223 (2015). [doi:10.1038/nature14066](https://doi.org/10.1038/nature14066) [Medline](#)
  35. L. Zhong, Y. Zhang, C. A. Duan, J. Deng, J. Pan, N. L. Xu, Causal contributions of parietal cortex to perceptual decision-making during stimulus categorization. *Nat. Neurosci.* **22**, 963–973 (2019). [doi:10.1038/s41593-019-0383-6](https://doi.org/10.1038/s41593-019-0383-6) [Medline](#)
  36. Y. Zhou, D. J. Freedman, Data and analysis code for: Posterior parietal cortex plays a causal role in perceptual and categorical decisions, Figshare (2019); <https://doi.org/10.6084/m9.figshare.8283251>
  37. W. F. Asaad, N. Santhanam, S. McClellan, D. J. Freedman, High-performance execution of psychophysical tasks with complex visual stimuli in MATLAB. *J. Neurophysiol.* **109**, 249–260 (2013). [doi:10.1152/jn.00527.2012](https://doi.org/10.1152/jn.00527.2012) [Medline](#)
  38. S. Bennur, J. I. Gold, Distinct representations of a perceptual decision and the associated oculomotor plan in the monkey lateral intraparietal area. *J. Neurosci.* **31**, 913–921 (2011). [doi:10.1523/JNEUROSCI.4417-10.2011](https://doi.org/10.1523/JNEUROSCI.4417-10.2011) [Medline](#)
  39. R. Ratcliff, G. McKoon, The diffusion decision model: Theory and data for two-choice decision tasks. *Neural Comput.* **20**, 873–922 (2008). [doi:10.1162/neco.2008.12-06-420](https://doi.org/10.1162/neco.2008.12-06-420) [Medline](#)
  40. R. Ratcliff, P. L. Smith, A comparison of sequential sampling models for two-choice reaction time. *Psychol. Rev.* **111**, 333–367 (2004). [doi:10.1037/0033-295X.111.2.333](https://doi.org/10.1037/0033-295X.111.2.333) [Medline](#)
  41. R. Ratcliff, J. N. Rouder, Modeling response times for two-choice decisions. *Psychol. Sci.* **9**, 347–356 (1998). [doi:10.1111/1467-9280.00067](https://doi.org/10.1111/1467-9280.00067)
  42. J. Vandekerckhove, F. Tuerlinckx, Diffusion model analysis with MATLAB: A DMAT primer. *Behav. Res. Methods* **40**, 61–72 (2008). [doi:10.3758/BRM.40.1.61](https://doi.org/10.3758/BRM.40.1.61) [Medline](#)
  43. Y. Zhou, Y. Liu, H. Lu, S. Wu, M. Zhang, Neuronal representation of saccadic error in macaque posterior parietal cortex (PPC). *eLife* **5**, e10912 (2016). [doi:10.7554/eLife.10912](https://doi.org/10.7554/eLife.10912) [Medline](#)

44. Y. Zhou, Y. Liu, S. Wu, M. Zhang, Neuronal Representation of the Saccadic Timing Signals in Macaque Lateral Intraparietal Area. *Cereb. Cortex* **28**, 2887–2900 (2018).  
[doi:10.1093/cercor/bhx166](https://doi.org/10.1093/cercor/bhx166) [Medline](#)
45. T. M. Herrington, N. Y. Masse, K. J. Hachmeh, J. E. T. Smith, J. A. Assad, E. P. Cook, The effect of microsaccades on the correlation between neural activity and behavior in middle temporal, ventral intraparietal, and lateral intraparietal areas. *J. Neurosci.* **29**, 5793–5805 (2009). [doi:10.1523/JNEUROSCI.4412-08.2009](https://doi.org/10.1523/JNEUROSCI.4412-08.2009) [Medline](#)
46. S. Martinez-Conde, S. L. Macknik, D. H. Hubel, Microsaccadic eye movements and firing of single cells in the striate cortex of macaque monkeys. *Nat. Neurosci.* **3**, 251–258 (2000).  
[doi:10.1038/72961](https://doi.org/10.1038/72961) [Medline](#)